Activation-dependent spatial dynamics of postsynaptic glycine receptors

Yoshihisa Nakahata

DOCTOR OF PHILOSOPHY

Department of Physiological Sciences

School of Life Science

The Graduate University for Advanced Studies

(SOKENDAI)

2013

Table of Contents

Abstract

Glycine is a major inhibitory neurotransmitter in the spinal cord and the brainstem. A glycine-mediated inhibitory neurotransmission (glycinergic transmission) is responsible for physiological functions that include motor control, afferent sensory transduction, visual and auditory transductions. Disruptions of glycinergic transmission caused by mutations to glycine receptors (GlyRs) are associated with hyperekplexia (so-called "startle disease"). Despite the physiological importance of glycinergic transmission, the primary mechanism of glycinergic synapse formation is still not fully elucidated.

The clustering of postsynaptic glycine receptors is considered to be established at immature stages by depolarization mediated increase in Ca^{2+}, and is disturbed by the chronic presence of strychnine, a selective glycine receptor antagonist. In mature neurons, however, the neuronal response to glycine receptor activation is the opposite, a hyperpolarization. Thus, glycinergic inputs evoke depolarizing responses at immature stage, but hyperpolarizing responses at mature stage due to the developmental upregulation of KCC2, an intracellular Cl^- extruder. The timing of this glycine-induced depolarizing to hyperpolarizing switch occurs at around the 1st postnatal week in mice and rats. Nevertheless, remodeling of inhibitory glycinergic synapses continues in the mature neuronal system. Therefore, the basic hypothesis that GlyR activation regulates

its localization at synapses in mature neuronal system needs investigation.

In this study, I have analyzed whether GlyR activation is responsible for synaptic localization and neurotransmission in mature cultured spinal cord neurons. To elucidate this question, I applied various experimental techniques to quantify GlyRs in neurons and synapses: conventional immunostaining, dynamic imaging techniques on living cells including fluorescence recovery after photobleaching (FRAP), combinations of fluorescence loss in photobleaching (FLIP), and a single particle tracking. Finally, I combined these with the voltage-clamp configurations of electrophysiological patch clamp recordings to measure functional synaptic transmission.

Primary cultures of spinal cord neurons were prepared from wildtype Wistar rats at embryonic day 14 (E14) for immunocytochemistry; from VGAT-Venus transgenic C57BL/6 mice E13-15 for single particle tracking; and from wildtype C57BL/6J mice E13-15 for FRAP, FRAP-FLIP and electrophysiological experiments. All procedures carried out in this study were approved by the Okazaki Institutional Animal Care and Use Committee, and conducted in accorded with guidelines defined by the National Institute of Natural Sciences. All the efforts were made to minimize suffering and the number of animals used in this study. Procedures of primary cultured neurons were mostly similar to standard protocols for primary hippocampal neurons.

In most of the present studies, three set of groups were compared. One was chronically treated with strychnine (1 µM final concentration, cSTR) to block GlyR

activation from the first day of culture. The second group (WASH) had one hour GlyR

activation by removing chronically applied strychnine only one hour prior to each

experiment. The third group (control) was incubated without strychnine from the first

day of culture plating. All the neurons were incubated on polyethylenimine-coated cover

glasses with Neurobasal medium at 37 °C and 5% CO_2 for 14-42 days in vitro (div).

To examine whether chronic blockade of GlyR affects its synaptic localization,

immunostaining was performed in control, cSTR and WASH groups. The results

showed that chronic strychnine caused a significant decrease in the intensity of GlyR

staining at synapses. The result of surface cell assay showed intracellular GlyR

expression was increased in cSTR compared with control group, but the total surface

expression that includes synaptic and extrasynaptic GlyRs was similar in each group.

These results indicated that GlyRs on the neuronal membrane are diffused away from

synapses in cSTR. Thus, I next examined GlyR dynamics in living neuronal culture by

using FRAP and FRAP-FLIP experiments, using a pH-sensitive GFP (superecliptic

pHluorin: SEP)-tagged GlyR to specifically visualize cell surface GlyRs.

This GFP-tagged GlyRα1 was firstly constructed, then transfected to cultured

spinal cord neurons by Lipofectamine 2000 at 13-15 days in vitro, with experiments

conducted within 48 hours after transfection. The results from the FRAP experiments

suggested that GlyR activation is responsible for its surface mobility. To distinguish

contributions of exocytosis, insertions from intracellular stores, and lateral diffusion on

the surface mobility, I performed a combination of FRAP-FLIP experiments. The result demonstrated that chronic blockade of GlyR induces an increase in the lateral diffusion of cell surface GlyRs without effects on GlyR exocytosis. In contrast, one hour GlyR activation (WASH group) was sufficient to reduce this change in diffusion properties in mature neurons.

For distinguishing GlyR lateral diffusion at synaptic vs. extrasynaptic location, mCherry-gephyrin (the postsynaptic scaffolding protein of GlyR) was cotransfected into neuronal cultures and focal FRAP (1 μm diameter) was performed at mCherry-expressed synaptic regions. The results showed that synaptic GlyRs had a significantly lower lateral diffusion following the activation of GlyRs. To quantify activation-dependent GlyR diffusion at synaptic and extrasynaptic locations, single particle tracking quantum dot-labeled GlyRs was employed, with FM 4-64 used to identify active presynaptic sites. The results indicated that laterally diffusing GlyRs stay for longer dwell times at synapse following GlyR activation.

Finally, I examined whether functional glycinergic transmission was modulated by chronic GlyR block using electrophysiological patch-clamp techniques. After activation of chronically blocked GlyRs, the amplitude of spontaneous miniature glycinergic currents was gradually increased after strychnine removal in cSTR group, but not in the control group. This supports the observations in live cell imaging that diffusion rate of synaptic GlyRs were decreased under the absence of strychnine. The

recording by gramicidin-perforated patch-clamp verified that the neurons used in the present study were mature, in terms of glycine-induced hyperpolarizations.

Overall, these results suggested that the activation of glycine receptor regulates the diffusion properties of the receptor and thereby functional glycine neurotransmission in mature neurons. Because glycine induces a hyperpolarization rather than depolarization in this matured stage, the previously proposed mechanism of glycinergic synapse formation at immature stage is insufficient to explain the results. Although the signaling mechanism is not fully elucidated, this is a novel report of activation-dependent glycinergic synapse formation in mature neurons.

Introduction

Excitatory and inhibitory neurotransmission are fundamental synaptic events in neural networks. Glycine is a major inhibitory neurotransmitter in the mature spinal cord and the brainstem where it on glycine mediates fast inhibitory transmission via activation of pentameric glycine receptor (GlyR) channels in mature neurons (Lynch, 2004). During development, the subunit composition of GlyRs changes from an α2 homomer to an α1β heteromer. The β subunit is capable to localize GlyRs at synapses by interacting with gephyrin, the inhibitory postsynaptic scaffolding protein (Meyer et al., 1995).

In the ventral horn of the spinal cord, glycinergic transmission mediated by Renshaw cells plays an important role for recurrent inhibition of motor neurons (Alvarez & Fyffe, 2007). Glycinergic synapses are essential for light modulation in retinal amacrine cells (Wässle et al., 2009) and sound localization in the lateral superior olive (LSO) nucleus of the brainstem (Sanes et al., 1998). In addition, glycinergic inhibitory transmission plays important role in modulating the ascending nociceptive pathway, and is considered as a novel therapeutic targets (Lynch & Callister, 2006). The disruptions of glycinergic transmission caused by mutations of GlyRs are associated with hyperekplexia (so-called "startle disease") (Dutertre et al., 2012). Thus, the glycine-mediating inhibitory neurotransmission is responsible for a variety of

physiological functions, including the development of neural networks (McDearmid et al., 2006).

At GABA-glycine mixed synapses in the lateral superior olive (LSO) of the brainstem, GABA is the presynaptically-released dominant neurotransmitters at early postnatal stage, with the proportion of glycine increasing in development (Nabekura et al., 2004). Correspondingly, expression of mature type synaptic α1 GlyR subunit (Friauf et al., 1997) and its mRNA (Piechotta et al., 2001) also increases in developing animals, at least until the 3rd postnatal week in LSO. Therefore, the corresponding increase of glycine and GlyRs have same time course in development. Indeed, previous studies using immunocytochemical staining reported that the blockade of GlyR activation by strychnine, and the blockade of neural activity by TTX, increases both the intracellular aggregations of GlyRs and decreases the synaptic membrane clustering of GlyRs (Lévi et al., 1998; Kirsch & Betz, 1998).

This synaptic GlyR clustering was explained by a model in which GlyR activation induces a depolarization due to the relatively high concentrations of intracellular Cl^- in immature neurons (Kakazu et al., 1999; Ben-Ari et al., 2007). The depolarization leads to Ca^{2+} influx via L-type Ca^{2+} channels (Kirsch & Betz, 1998) and N-methyl-D-aspartic acid (NMDA) receptors (Lévi et al., 2008). Then, intracellular Ca^{2+} elevation facilitates GlyR interaction with gephyrin, the scaffolding protein for GlyRs at synapses (Kirsch & Betz, 1998). Further studies also suggested that activity of

7

calcium-calmodulin-dependent protein kinase II (CaMKII) enhance GlyR clustering

(Charrier et al., 2010; Yamanaka et al., 2013), while the increase of protein kinase C

(PKC) activity decreases interactions of GlyR and gephyrin. (Specht et al., 2011).

However, the GlyR-mediating response shifts from a depolarization to a

hyperpolarization (D-H shift) due to a developmental increase of KCC2 expression, an

intracellular Cl^- extruder, after the first postnatal week (Ben-Ari, 2002). While the

response to glycinergic transmission induces hyperpolarization after the first postnatal

week, an increased GlyRα1 and upregulated proportion of presynaptic glycine release

was detected even at the 3rd postnatal week. Although the proposed GlyR-mediating

depolarization induced GlyR clustering is conceivable at immature stage, this model is

insufficient to explain developmental increases of mRNA and protein of synaptic

GlyRα1 after the first postnatal week (Friauf et al., 1997; Piechotta et al., 2001). The

formation of appropriate glycinergic synapses is essential for various physiological

functions, yet the primary mechanism of glycinergic synapse formation is still not fully

elucidated. The question therefore arises as to whether GlyR activation is responsible

for the formation of postsynaptic GlyRs clustering in mature spinal cord and brain stem

neurons, at a time when glycine transmission is hyperpolarization.

To elucidate this question, I investigated activation-dependent localization and

dynamics of synaptic GlyRs, and functional neurotransmission in cultured spinal cord

neurons. I found that the activation of glycine receptors decreases their lateral diffusion

at synapses. The functional correlate of this phenomenon was observed as increased miniature glycinergic IPSCs amplitude. The formation of glycinergic synapse was considered to occur only at immature stage; however, I found here that GlyR activation induces synaptic clustering even in the mature neurons. While the signaling mechanism was not fully elucidated, this is a novel report underlying the activation-dependent glycinergic synapse formation in mature neurons.

Experimental Procedures

All procedures carried out in this study were approved by the Okazaki Institutional Animal Care and Use Committee, and conducted in accorded with guidelines defined by the National Institute of Natural Sciences. All the efforts were made to minimize suffering and the number of animals used in this study.

Primary spinal cord culture

Primary cultures of spinal cord neurons were prepared from wildtype Wistar rats at embryonic day 14 (E14) for immunocytochemistry; from VGAT-Venus transgenic C57BL/6 mice E13-15 for single particle tracking; and from wildtype C57BL/6J mice E13-15 for FRAP, FRAP-FLIP and electrophysiological experiments. Embryos were isolated from pregnant animals under isoflurane anesthesia, and immediately placed into ice-cold Leibovitz's L-15 medium (Life Technologies, Tokyo, Japan). Their spinal cords were quickly removed and incubated in HEPES-buffered Dulbecco's Modified Eagle's Medium (HDMEM) containing papain (24 µl/ml; Worthington, Lakeland, NJ, USA), S1, BSA, penicillin/streptomycin, EDTA and L-cysteine for 20 min at 32 ℃. Then individual cells were dissociated by repeated trituration using pipettes in Neurobasal medium containing DNase and L-glutamate. Healthy cells were collected by centrifugation at 8,000 rpm for 1 minute, and the

supernatant was exchanged with Neurobasal medium containing B27 supplement and Glutamax (Life Technologies, Tokyo, Japan), penicillin 100 U/ml and streptomycin 100 μg/ml. Cells were plated on either polyethylenimine-coated 18 mm diameter or 8 x 8 mm cover glass (Matsunami, Osaka, Japan) at a density of 1.0-1.6 x 10^4 cells/cm^2, and incubated at 37 °C and 5% CO_2 for 14-42 days before experiments.

Three set of groups were compared in the present study (Fig. 1A). One was chronically treated with strychnine (1 μM final concentration, cSTR) to block GlyR activation from the first day of culture. The second group (WASH) had one hour GlyR activation by removing chronically applied strychnine only one hour prior to each experiment. The third group (control) was incubated without strychnine from the first day of culture plating.

DNA Constructs and transfection

Superecliptic pHluorin (Gift from Dr. G. Miesenböck, Univ. of Oxford) was designed to be translated within the extracellular domain of the mouse GlyRα1 subunit (Kindly provided by Dr. H. Hirata, National Institute of Genetics) following signal peptide sequences (pCAG-SEP-GlyRα1; Fig. 3A). mCherry-gephyrin construct was kindly provided by Dr. T. Kuriu (Tokushima Bunri Univ.). Briefly, gephyrin-P1 splice variant 1 of rat was N-terminally labeled with mCherry (Fig. 6A) (Kuriu et al., 2012). Cells were transfected 13-15 days after plating and imaged within 48 hours after

transfections. Transfections were performed using Lipofectamine 2000 (Life Technologies, Tokyo, Japan) in Neurobasal medium lacking penicillin/Streptomycin for 6-8 hours.

Reagents

Drugs used in the present study were DL-2-amino-5-phosphonopentanoic acid (AP-V), 6-cyano-7-nitroquinoxaline-2,3-dione (CNQX), 6-imino-3-(4-methoxyphenyl)-1(6*H*)-pyridazinebutanoic acid (SR95531), strychnine, gramicidin D, glycine (All from Sigma-Aldrich Japan, Tokyo, Japan), and TTX (Latoxan, Valence, France). Drug-contained solutions were locally applied via a Y-tube system (Murase et al., 1989) in electrophysiological recordings, and bath-applied in imaging experiments.

Solutions

The standard extracellular solution contained (in mM): 148 NaCl, 5 KCl, 1 $MgCl_2$, 2 $CaCl_2$, 10 glucose, 10 hydroxyethyl-piperazine-*N*-2-ethanesulphonic acid (HEPES) and adjusted to pH 7.4 with Tris-OH. In all experiments, the standard extracellular solution contained (in μM) 5 CNQX, 5 AP-V, 1 SR95531, 0.3 TTX. Additionally, 1 μM strychnine was constantly present in cSTR group, and present in WASH group until one hour before recording. Quantum dot (QD) binding buffer

contained (in mM) 2.62 sodium tetraborate decahydrate, 39.5 boric acid and 2% (w/v) bovine serum albumin and adjusted to pH 7.4 with 1 M HCl or 1 M NaOH. In electrophysiological experiments, the internal pipette solution for the perforated-patch clamp configuration contained (in mM): 90 KCl, 60 K-methansulfonate, 10 HEPES. The pipette solution for conventional whole-cell configuration contained (in mM): 100 K-methanesulfonate, 8 NaCl, 30 KCl, 1 $MgCl_2$, 2 EGTA, 4 Mg-ATP, 5 QX-314-Cl, 10 HEPES. All pipette solutions were adjusted to pH 7.3 with Tris-OH. In perforated-patch clamp configuration, gramicidin D was initially dissolved in DMSO at 10 mg/ml and then diluted to a final concentration of 20-40 µg/ml in the pipette solution. The gramicidin was prepared just before use.

Immunocytochemistry, image acquisition and quantitative analysis

Cultured rat spinal cord neurons were fixed with paraformaldehyde (PFA, 4% w/v) in phosphate buffered saline (PBS) and then permeabilized with Triton X-100 (0.1%, v/v). Non-specific antibody binding sites were blocked with PBS containing normal goat serum (2%, v/v) and bovine serum albumin (1%, w/v). Cells were double labeled with primary antibodies of polyclonal rabbit anti-VIAAT (1:500; Synaptic Systems 131 002) and monoclonal mouse anti-glycine receptor α1 (mAb2b; 1:200; Synaptic Systems 146 111) overnight at 4 °C, followed by incubation with fluorescence-conjugated secondary antibodies (Alexa Fluor 633, 1:1000; and Alexa

13

Fluor 488, 1:1000, Life Technologies Tokyo, Japan) for 30 minutes at room temperature.

Coverslips were mounted in PermaFluor aqueous mounting medium (Thermo Shandon,

Pittsburgh, PA). Fluorescence images were acquired with a confocal laser scanning

microscope (Nikon A1, Plan Apo-VC 100x H, NA 1.4, Tokyo, Japan). Pixel size and

focus steps were of 0.1 μm and 0.37 μm, respectively, with images of 1024 x 1024

pixels. GlyRα1 signals overlapped (at least one pixel) with VIAAT signals were

considered to be colocalized.

Cell Surface Biotinylation

Surface biotinylation experiments were performed using a cell surface protein

biotinylation and purification kit (Pierce) according to the manufacturer's protocol.

Briefly, cultured spinal cord neurons from four individual cultures (div19-33) were

washed with ice-cold PBS and then labeled with 0.25 mg/ml sulfo-NHS-SS-biotin for

30 min at 4 °C before washing with PBS supplemented with quenching solution to

remove excess biotin. The cell lysates were centrifuged (10,000 x g, 2 min), the

supernatant was isolated with NeutrAvidin gel, and the bound proteins were then eluted

with SDS sample buffer (62.5 mM Tris-HCl, pH 6.8, 1% SDS, 10% glycerol) and

analyzed by SDS-PAGE and Western blotting.

Immunoblotting

Proteins were separated using 7.5% acrylamide gels by SDS-PAGE. The gels were transferred to an Immobilon-P membrane (Millipore, Bedford, MA). The blots were blocked in 1% bovine serum albumin and incubated overnight with primary antibody at 4 °C. They were then incubated with horseradish peroxidase-conjugated secondary antibody (GE Healthcare UK Ltd., Buckinghamshire, England) for 1 h at room temperature. Enhanced chemiluminescence (ECL, GE Healthcare) exposure on instant film and an ECL mini-camera luminometer were used to visualize labeled protein. The following primary antibodies were used: anti-pan GlyRs (mAb4a; 1:1000, Synaptic Systems), anti-actin (1:10,000; Sigma-Aldrich). The optical densities of bands were analyzed with Scion Image software with a gel-plotting macro program. The total GlyR band density was normalized to the actin band density.

Fluorescence recovery after photobleaching (FRAP) and fluorescence loss in photobleaching (FLIP)

For experiments applying fluorescence recovery after photobleaching (FRAP) and fluorescence loss in photobleaching (FLIP) (Hildick et al., 2012), mouse spinal cord neurons (13-15 div) were transfected with pCAG-SEP-GlyRα1 and CMV-mCherry-Gephyrin construct(s) at 24-48h prior to experiments. Imaging was performed at room temperature (24 ± 2 ºC) in 5 mM K$^+$ standard recording solution. Images were acquired with a confocal laser scanning microscope (Nikon A1, Plan

15

Apo-VC 60x H, NA 1.4, Tokyo, Japan). Fluorescence was photobleached using 488-nm laser at a full power of 40 mW for 62.5 ms for 7 times in two 3 x 5 μm rectangular regions of interests (ROIs) at SEP-expressed neurites. For the focal FRAP protocol, photobleaching was applied to 1 μm diameter circular ROIs were applied at with and without mCherry-expressed puncta. Laser power at 1% was used for image acquisitions.

In FRAP-FLIP protocol, continuous photobleaching at the FLIP regions (3 x 5 μm rectangles at each side of the FRAP region) gradually decreases the intensity of the FRAP ROI. This signal may be due to slight leakage of stimulation light into the FRAP region, or due to bleached SEP-GlyR entering into the FRAP region, thus the initial bleaching region was expanded (10 x 5 μm) and FLIP ROIs were set along the edges of the enlarged initial bleaching region (Fig. 5A). For comparison with non-FRAP-FLIP (FRAP-only) protocol, the same size of FRAP ROI (3 x 5 μm) was measured in the center of the enlarged initial bleaching region. If exocytosis of SEP-GlyRs was a major factor for fluorescence recovery, recovery rates in FRAP-FLIP protocol should be similar to the rates in the FRAP-only protocol. In both FRAP and FRAP-FLIP experiments, image acquisitions were performed 90 times with three seconds intervals (total 270 seconds). Fluorescence recovery was measured after a correction based on the intensities of unbleached regions. Recovery rates were calculated by normalizing by average values of three prebleaching intensities.

Live cell staining

Firstly, once washed with Neurobasal medium, neurons were incubated for 5 minutes with primary antibody which recognizes an extracellular epitope of the GlyRα1 subunit (5 µg/ml, mAb2b, Synaptic systems, Göttingen, Germany), then washed 5 times. Secondly, they were incubated for 5 minutes with secondary antibody (5.2 µg/ml; biotin Fab goat anti-mouse IgG (H+L), Jackson ImmunoResearch, West Grove, USA), then washed 5 times again. Reactions of primary and secondary antibodies and washing were performed in Neurobasal medium. Thirdly, the neurons were incubated with streptavidin-conjugated quantum dots emitting at 605 nm (1 nM; Life Technologies, Tokyo, Japan) in QD binding buffer (Bannai et al., 2006) for 1 minute. After washing 8 times with 5 mM KCl standard imaging solution, they were incubated with FM4-64 (2 µM; Life Technologies, Tokyo, Japan) in 40 mM KCl standard solution for 30 seconds to label active presynaptic sides (Gaffield & Betz, 2007). Live cell staining and washing processes were performed at 37 ºC.

Single particle tracking

QD-labeled neurons were imaged in the standard recording solution. Using an inverted microscopy (IX70, Olympus, Tokyo, Japan) equipped with an oil-immersion objective (100x, NA 1.4), EM-CCD camera (ImagEM C9100-13, Hamamatsu Photonics), mercury lamp, appropriate band pass filter sets for QD 605 (ex. 457/50 and

em.605/15), FM4-64 (ex. 510/84 and em.736/128), Venus (ex. 457/50 and em.530/55). Single images of FM4-64 and Venus were taken before the QD imaging. QD movies of 300 frames were then recorded at 66.7 ms acquisition rates at 33.3 ms intervals with MetaMorph software v7.7 (Molecular Devices, Sunnyvale, USA). The movements of QD-GlyRα1s were recorded within 45 minutes after labeling. Each solution contained AP-V (5 µM), CNQX (5 µM), SR95531 (1 µM), TTX (0.3 µM) except 40 mM KCl solution, and strychnine (1 µM) was only in the cSTR group during staining and imaging.

Electrophysiological measurements

Cultured neurons were viewed under phase contrast on an inverted microscope (IX70, Olympus, Tokyo, Japan). Ionic currents were measured with a patch-clamp amplifier Multiclamp 700B (Axon Instruments, Union City, CA, USA), and recorded with a sampling frequency of 20 kHz after low-pass filtering at 5 kHz. Currents were recorded, and voltage protocols were applied, using pClamp 10.2 software (Molecular Devices, Sunnyvale, USA). The resistance between the patch pipette filled with the internal solution and the reference electrode in the standard external solution was 6−8MΩ. The neurons were voltage-clamped at a holding potential (Vh) of −50 mV in gramicidin-perforated patch experiments and −70 mV in the conventional whole-cell patch-clamp configurations.

The reversal potentials of glycine-induced currents (E_{gly}) were recorded using gramicidin-perorated patch configurations to maintain intracellular Cl$^-$ concentrations intact (Ebihara et al., 1995). Voltage-ramps from -110 to $+40$ mV duration 1.6 seconds were applied to the neuron before and during glycine application. Voltage protocols were generated by a software-driven digital-to-analog converter (Digidata 1322A, Molecular Devices). Corrections for liquid junction potential (0.8 mV) was applied to the data in gramicidin-perforated recordings. Current-voltage (I-V) relationships were measured by subtracting current values during the control from those during glycine application. Each E_{gly} was quantified as the intersections with the horizontal axis.

Spontaneous miniature glycinergic currents (miniature I_{gly}) were recorded using conventional whole-cell patch-clamp configuration. To measure miniature I_{gly}, chronically treated strychnine must be removed, thus the bath solution including strychnine was completely exchanged to the standard recording solution lacking strychnine immediately before recording in cSTR group. In control group, the bath solution was completely exchanged to the solution including 1 μM strychnine for 30 seconds and then quickly exchanged again to the standard solution lacking strychnine in order to exclude the effect of any residual strychnine between control and chronic strychnine treatment groups (Fig. 13A). Recordings started within 10 minutes after strychnine washout and lasted for 60 minutes. Miniature I_{gly} were confirmed by application of 1 μM strychnine after each recording.

In all electrophysiological experiments, standard recording solutions contained 5 µM CNQX, 5 µM AP-V, 1µM SR95531 and 0.3 µM tetrodotoxin (TTX). Under these conditions, spontaneous excitatory and GABAergic postsynaptic currents and action potentials were fully inhibited. All experiments were carried out at room temperature (21−24ºC). Recordings were discontinued if the access resistance changed markedly.

Data analysis

All data are presented as mean ± SEM. Differences between groups were analyzed for statistical significance using a two-tailed Student's *t* test for two groups, and one-way ANOVA with Dunnett's multiple comparison post hoc test for multiple groups. The level of significance was set at $*p < 0.05$, $**p < 0.01$, $***p < 0.001$ for all tests.

For single particle tracking, QD-GlyR particles located on the Venus-expressing neurons were only used for analysis to exclude non-specific signals. The trajectory of each particle was determined by cross-correlating the image with a Gaussian model of the point spread function (Bonneau et al., 2005), using TI workbench software written by T. Inoue (Waseda Univ.) (Bannai et al., 2009). Only single QDs identified by their characteristic blinking were analyzed to avoid false positive noises (Single QD-GlyRs recorded for more than 295 frames were excluded from analysis). The synaptic areas were defined by processing FM4-64 images with

top-hat filtering (Waataja et al., 2008). In each frame, QD-GlyR merged at least 1 pixel with binalized image of FM 4-64 was defined as synaptic and more than 2 pixels away from the FM 4-64 image was defined as extrasynaptic. For the calculation of diffusion parameters in the synapse (except for synaptic dwell time), the longest sub-trajectories (segments) of single QD-GlyRs that consisted of more than or equal to 30 frames in each compartment, were considered to be representative of each particle's behavior in that compartment.

To obtain the diffusion coefficients, values of the mean square displacement (MSD) plot versus time were calculated for each trajectory by applying the following equation:

$$MSD(n\tau) = \frac{1}{N-n}$$
$$\sum_{i=1}^{N-n}[(x((i+n)\tau) - x(i\tau))^2 + (y((i+n)\tau) - y(i\tau))^2]$$

where τ is the acquisition time, N is the total number of frames, and n and i are positive integers with n representing the time increment. Diffusion coefficients (D) were calculated by fitting first three points of the MSD versus time curves with the following equation:

$$MSD(n\tau) = 4Dn\tau + b$$

where b is a constant reflecting the spot localization accuracy. The dwell time of QD-GlyR inside the synapse was defined as the duration of synaptic location.

Results

Chronic blockade of glycine receptors decreases their localization at synapses

Localization of glycine receptor α1 subunits (GlyRα1) at synapses was investigated in cultured neurons of wildtype rat spinal cord with double-immunolabeling experiments using antibodies against GlyRα1 and VIAAT (VGAT), an inhibitory neuron presynaptic terminal marker. VIAAT signals were densely observed opposed to neuronal somata (Fig. 1B2, C2, D2) and punctate signals of GlyRα1 were detected along the surface of neurons (Fig. 1B3, C3, D3). A colocalization index of GlyRα1 at inhibitory synapses were measured to compare between the groups. Almost the half of glycine receptors were apposed to VIAAT positive presynapses in control (0.49±0.04), and this proportion of synaptic GlyRα1 was similar in WASH group (0.53±0.02) (Fig. 1E). However, chronic application of strychnine significantly decreased GlyRα1 at synapses (0.31±0.01, $p < 0.01$) (Fig. 1E).

Chronic blockade of glycine receptors does not seem to alter the surface expression of glycine receptors

Previous studies reported that chronic strychnine treatment decreased synaptic GlyRs and increased internal GlyR aggregates (Lévi et al., 1998; Kirsch and Betz, 1998). To quantify GlyR expression levels on the surface as compared to total neuronal

expression, surface biotinylation assay was performed. Due to difficulties of culturing

sufficient amount of spinal cord neurons, I could not generate a sufficient sample size to

allow statistical analysis, but the preliminary result suggested the amount of GlyRs (α1,

α2, α3, and α4) expressed in the cell surface in cSTR group was similar to that of

control (and WASH) (Fig. 2A & B). However, the total expression level of GlyRs

seemed higher in cSTR and WASH groups than that of control level (Fig. 2A & B).

Dynamic GlyR mobility on the cytoplasmic membrane

Recent technical advancements in live cell imaging revealed that the

localization of membrane receptors is not static, but dynamic (Ashby et al., 2006).

Therefore, live cell imaging applying fluorescence recovery after photobleaching

(FRAP) was used to elucidate dynamic movement of GlyRs (Soumpasis, 1983; Reits &

Neefjes, 2001). The GlyRs located on the cytoplasmic membrane may be activated by

their ligand, thus it is necessary to distinguish the receptors located on the cell surface

and in the cytoplasm. For selective visualization of surface GlyRs, superecliptic

pHluorin (SEP), a pH-sensitive derivative of EGFP was applied to this experiment

(Miesenböck et al., 1998; Ashby et al., 2004). SEP protonation decreases its absorption

rate and therefore decreases its fluorescence emission rate at the low pH (pH 5), found

in secretory vesicles in the cytoplasm (Ashby et al., 2004). However, it effectively emits

fluorescence around pH 7 (Fig. 3B). Sankaranarayanan et al., (2001) suggested that SEP

fluorescence is 21 times brighter at pH 7.4 than at pH 5.5, so construction of SEP-tagged GlyRα1 allows selective visualization of GlyRα1 presenting in the cellular membrane (Fig. 3C).

To examine the effect of glycine receptor activation in its mobility on the cell surface, I made a pCAG-SEP-GlyRα1 (Fig. 3A) constructed and transfected in the cultured neurons. Since the volume of the bleaching region may affect its fluorescence recovery rate, neurites with a similar width were randomly selected and compared in each groups (Fig. 4A). There was very little fluorescence recovery in the bleached region in the control group, while a rapid fluorescence recovery was seen in the cSTR group after bleaching, with this recovery rate gradually slowing down during the later phase in the measurement (Fig. 4B). One hour after removal of chronic strychnine in the WASH group the recovery rate (Fig. 4B, light blue, 0.05 ± 0.02, n=5) was very low and similar to control level (Fig. 4B, black, 0.07 ± 0.02, n=7). The average recovery rates in the last ten seconds of each recording were statistically compared between the groups (yellow colored points in Fig. 4B), and cSTR group (Fig. 4B, magenta, 0.45 ± 0.02, n=7) showed a significantly higher recovery rate than both control and WASH groups (Fig. 4C; ***$p < 0.001$, n=5-7).

Higher recovery rate at the bleached region in chronic strychnine treatment indicated the presence of newly appearing GlyRs in the bleached regions that may be due to either exocytosis of GlyRs from cytoplasmic secretory vesicles or laterally

diffusion of receptors from outside the bleached region (Fig. 3C). To distinguish these, brefeldin A (BFA: an inhibitor of ER-golgi transport that results in exocytosis inhibition) was applied to the group treated strychnine (cSTR+BFA) (Rannals, 2011). BFA application did not significantly affects the higher fluorescence recovery rates seen with chronic strychnine treatment, indicating that fluorescence recovery is not likely to be due to exocytosis (Fig. 4C).

However, I suggest fluorescence recovery is due to in response to removal of chronically applied strychnine. To confirm this, the fluorescence loss in photobleaching (FLIP) configuration was combined with FRAP experiment (Fig. 5A) (Hildick et al., 2012). Continuous photobleaching (FLIP) of the regions outside the FRAP ROI, can bleach the fluorescence signals of GlyRs in the membrane to rule out the fluorescence recovery due to laterally diffusing SEP-GlyRs. In this FRAP-FLIP configuration, the fluorescence recovery indicates newly exocytosed SEP-GlyRs at FRAP area. In both control and WASH groups fluorescence recovery rates were again very slow and they were similar to those in FRAP-only configuration (Fig. 5B & C). On the contrary, the fluorescence recovery rate in FRAP-FLIP decreased when compared to FRAP-only protocol in the chronic presence of strychnine group, confirming that the decreased proportion of fluorescence recovery is due to lateral diffusion (Fig. 5B & C). Moreover, the fluorescence recovery rate in cSTR group became the same level as that in control and WASH groups (Fig. 5B & C). Overall, these results indicate that

activation-dependent GlyR mobility may be due to changing properties of lateral diffusion.

Dynamic mobility at the presence of postsynaptic scaffolding protein

Next I examined whether the activation-dependent mobility shift is observed at the postsynaptic membrane where synapse scaffolding protein exists. Because the lack of a specific glycinergic synapse marker, mCherry-tagged gephyrin, the postsynaptic scaffolding protein at inhibitory synapses, was used to identify the potential postsynaptic structures (Meier et al., 2001). mCherry-gephyrin construct was cotransfected with SEP-GlyRα1 (Fig. 6A & B). mCherry-gephyrin showed punctate signals in neural processes, (so focal photobleaching of 1 μm diameter was performed on these distinctive punctate spots (defined as synapses) and on regions with no signal (defined as extrasynapse) (Fig. 6B). Fluorescence recovery was higher at gephyrin-lacking regions than at gephyrin-positive regions in control ($p < 0.001$, n=14) and WASH ($p < 0.001$, n=15) groups (Fig. 6C, D & E). At gephyrin positive spots, both control and WASH groups showed similar fluorescence recovery rates. In contrast, cSTR groups showed much higher fluorescence recovery rates at gephyrin positive spots (Fig. 6E). Therefore these results suggest that the activation-dependent dynamic changes of GlyR mobility were observed at potential synaptic sites.

Higher mobility by strychnine treatment is independent of neural activity during development

Strychnine is a potent competitive antagonist of glycine receptors; therefore chronic strychnine application may cause disinhibition and thus enhance neural activity during development of circuits in vitro. The possibility of such a cSTR-induced overexcitation may induce the higher mobility of GlyRα1. To address this question, recovery rates of fluorescence were measured at 1 µm diameter bleached synaptic spots in cultures with chronic application of cSTR+TTX 0.3 µM, and cSTR+AP-V 5 µM+CNQX 5 µM from the first day of culture. The recovery rates of these two groups showed no differences from those in the normal cSTR group, suggesting that higher GlyR mobility after chronic strychnine treatment is independent of neural activity (Fig. 7A & B). Whereas TTX application increased GlyRα1 lateral diffusion in a previous report (Lévi et al., 2008), the lateral mobility of GlyRα1 was not increased by additional application of TTX in the present experiments. This suggests that GlyRα1 mobility was already at a high plateau level with the chronic strychnine treatment, so TTX could not increase further.

The effect of strychnine on the previously activated glycine receptors

Because GlyRα1 showed higher diffusive property in the chronic presence of strychnine, the effect of GlyR blockade on GlyRs that had been previously activated

was analyzed by FRAP of 1 μm diameter at synapses. The same concentration of strychnine (1 μM) as cSTR group was applied to control conditions. For three different time points (STR 0h, STR 1h, and STR 24h; Fig. 8A) were examined. The results showed that recovery rates of fluorescence at the photobleached regions were significantly lower than in the chronic strychnine treatment (cSTR) in all three of these acute strychnine groups (Fig. 8B & C). The recovery rates were similar to control, suggesting no effect of strychnine. Immunohistochemical analysis previously reported that strychnine decreased already established GlyR clusters, but this effect was suppressed with development (Yamanaka et al., 2013). Thus these results suggest that the chronic blockade of GlyRs enable them with a high mobility, but once GlyRs have been activated their capacity for high lateral diffusion decreases. Later blockade for up to 24 hours of previously activated GlyR doesn't affect this mobility at synapses.

Potential mediator(s) of GlyR activation-dependent GlyR stabilization

Previous studies suggested that CaMKII activation (Yamanaka et al., 2013) and Ca^{2+} influx (Kirsch & Betz, 1998; Lévi et al., 2008) by GlyR activation-dependent depolarization mediates GlyR clustering at synapses. 10 μM KN62, a CaMKII inhibitor and, 10 μM BAPTA-AM, a Ca^{2+} chelator, were separately applied when strychnine was removed from the chronic strychnine treatment (WASH group) to investigate whether either Ca^{2+} elevation or CaMKII activity mediates the expression of activation-induced

GlyR stabilization at synapses. Fluorescence recoveries at synapses were measured by the focal FRAP protocol. However, both KN62 and BAPTA-AM had no effect on recovery curves as compare to WASH (Fig. 9A & B). Vaello et al., (1994) showed that protein kinase A (PKA) activity increases glycinergic current response ; therefore the effects of 100 μM Rp-cAMPs, a PKA inhibitor was also examined in the same way, while Rp-cAMP failed to suppress activation-dependent decreases of fluorescence recoveries (Fig. 9A & B). Although the concentrations of these inhibitors were sufficient to maximally inhibit their targets based on the previous studies, they were not effective to attenuate GlyR activation-dependent fluorescence recoveries. To examine contributions of the wide range of kinases more broadly, the effect of 10 μM staurosporine, a broad kinase inhibitor was assessed in the same manner. Even though GlyRs were activated after removal of strychnine, staurosporine caused a fluorescence recovery rate as high as the cSTR group. Hence a staurosporine-sensitive kinase may mediate the activation-dependent GlyR stabilization at synapses(Fig. 9A & B).

Single particle tracking of GlyR at synaptic sites

Interestingly, GlyRs labelled with fluorescent particles show dynamic diffusion on the neuronal surface, and enter and exit synapses in few seconds (Dahan et al., 2003; Lévi et al., 2008). To analyze the activation-dependent modulation of lateral diffusion of GlyRs, quantum dot (QD) live cell imaging was applied to cultured neurons. GlyRα1

was labeled by conjugation of a selective antibody against an extracellular epitope of GlyRα1 with streptavidin-coated QDs via biotinylated Fab fragment. Active presynapses were labeled by uptake of FM-4-64 (Fig. 10A). Mobile QD-conjugated GlyRα1 (QD-GlyRs) were recorded for 30 seconds (300 frames), and the signals merged with FM-4-64 were considered to be located at synapses (Bannai et al., 2006).

In order to exclude non-specific signals, single QD-GlyRs located in both synaptic and extrasynaptic areas were selected to be analyzed. Each QD-GlyR signal was tracked and used to calculate a diffusion coefficient (D ($\mu m^2/s$)), and the time spent in synaptic locations. In the control group, diffusion coefficients of each individual QD-GlyRs at synapse were significantly lower than those of extrasynaptic locations (Fig. 10B, $p < 0.05$, n=28). Figure 10D shows an example of instantaneous diffusion coefficients (D_{inst} ($\mu m^2/s$)) throughout 30 seconds recordings at synapse and extrasynaptic location in a control experiment (shown in Fig. 10C). The Diffusion coefficient was decreased when QD-GlyRs entered into a synaptic location. In contrast, changes in the instantaneous diffusion coefficient was varied, and not associated with synaptic locations, in the chronically strychnine treatment group (Fig. 10D, right panel).

The mean diffusion coefficients at synapses were not statistically different between control, cSTR and WASH groups. However, the individual diffusion coefficient values varied greatly, and the median values of control and WASH groups were relatively lower than that of cSTR condition (Fig. 11A). The dwell times of each

QD-GlyR at synapses were calculated based on the continuous set (segment) of time in which QD-GlyRs stayed at either synapse or extrasynapse. The majority of QD-GlyRs stayed at a synapse for 1.25 seconds in control, cSTR and WASH groups. However, the proportion of longer dwell times at synapse were smaller in cSTR than in control and WASH groups (Fig. 11B). The average dwell time in cSTR (2.7 ± 0.2 sec, n=314) was shorter than that of control (5.9 ± 0.7 sec, n=150, $p < 0.001$), while the average dwell time in WASH group (4.3 ± 0.7 sec, n=97) was similarly longer level as that of control (Fig. 11C). These results suggest that activation of glycine receptors decreases their lateral diffusion and causes them to stay for longer durations at synapses.

GlyR activation induces hyperpolarization

Glycine-induced depolarization is the initial step in the conventional model of activation-dependent GlyR clustering in immature neurons (Lévi et al., 1998; Kirsch & Betz, 1998). To determine in the present study using neurons cultured for 14-42 div whether glycinergic input induces depolarization or hyperpolarization, the reversal potentials of glycine-induced currents (E_{gly}) were measured by using the gramicidin-perforated patch-clamp configuration (Ebihara et al., 1995) in control and cSTR groups.

The application of glycine (100 µM) to cultured spinal cord neurons voltage clamped at a holding potential (V_h) of -50 mV consistently evoked outward currents in

31

both control and in cSTR groups (Fig. 12A). Voltage ramps revealed an exchange

current reversal potential (E_{gly}) were similar level in control (-71.6 ± 0.8 mV, n=6) and

cSTR (-68.0 ± 1.94 mV, n=5) groups (Fig. 12B). No differences in E_{gly} were detected

across the range of days in vitro (14-39 div). These results suggest that glycinergic input

is not depolarizing but hyperpolarizing response in both control and cSTR groups in the

present study.

Activation-dependent GlyR clustering in the synaptic transmission

Activation-dependent GlyR stabilization was so far analyzed by

immunocytochemical and live cell imaging techniques. Next, I examined whether those

dynamic structural changes modulated on the synaptic transmissions. In both control

and chronically strychnine treated (cSTR wash) groups, miniature glycinergic currents

(mI_{gly}) were measured using conventional whole-cell patch-clamp configuration

beginning within 10 minutes after strychnine removal (Fig. 13A, details written in

Methods). The voltage clamp recordings were performed in the presence of 0.3 μM

TTX, 5 μM AP-V, 5 μM CNQX, 1 μM SR95531, at a holding potential (V_h) of -70 mV.

Although the amplitude and frequency of mI_{gly} were varied in each neuron in

control and cSTR wash groups. They were nearly stable during 60 minutes recording in

control group (Fig. 13B upper, C left panel, D), while gradually increased in cSTR wash

group (Fig. 13B, C right panel & D). This was particularly evident for mI_{gly} amplitudes,

and the frequencies of miniature I_{gly} was not different between control and cSTR wash groups (Fig. 13E). The approximately constant miniature I_{gly} frequency over the 60 minutes recording indicates that chronic strychnine treatment did not affect presynaptic glycine releases (Fig. 13E). The increase of amplitude of miniature I_{gly} indicated that the number of glycine receptors seemed to increase at postsynaptic sites by activation of GlyRs after chronic strychnine removal.

As spontaneous mI_{gly}s were observed from the beginning of electrophysiological recordings without presence of exogenous glycine application (Fig. 13B), endogenous presynaptic glycine release was very likely occurred during the incubation. The complete inhibition of mI_{gly}s by 1 µM strychnine after in each recording also showed that 1 µM strychnine is a sufficient concentration to block GlyR activation by this endogenous synaptic glycine release.

Discussion

There are two main pathways directly regulating synaptic receptor localizations: exocytosis of preformed GlyRs in internal secretory vesicles fusing with the cytoplasmic membrane, and lateral diffusion of GlyRs from extrasynaptic locations in the cytoplasmic membrane (Borgdorff & Choquet, 2002). The current results demonstrate that modulating lateral diffusion is the main pathway for activation-dependent GlyRs localization. Previous studies initially suggested that chronic inhibitions of GlyR and/or neuronal activity results in GlyR intracellular aggregations (Lévi et al., 1998), and thus a decrease synaptic GlyRs (Kirsch & Betz, 1998). However, a further study revealed that the cytoplasmic GlyR aggregations are caused by disturbances of degradation mechanisms within the cytoplasmic residual pool, with the half-life of GlyR unchanged at the cell surface by strychnine (Rasmussen et al., 2002). The preliminary result of surface cell assays also implies that dislocation and restoration of GlyRs at synapses are not affected by surface expression of GlyRs. Thus, the present results suggest that GlyR activation increases synaptic localization of GlyRs by decreasing lateral diffusion, rather than by exocytosis (but this may makes small contribution).

Previous studies suggested that the enhanced neural activity and activation of NMDA receptors reduces lateral diffusion of GlyRs (Lévi et al., 2008; Charrier et al.,

2010) and thus increases synaptic localization (Kirsch & Betz, 1998; Lévi et al., 2008). According to those reports, it was possible that the increase in synaptic GlyR localization in cSTR group was due to an enhanced neuronal activity as a result of suppressing glycinergic transmission. However, GlyR mobility in cSTR group was higher, and with a lower synaptic localization, compared with those of control group. In addition, the results from experiments that chronically suppressed neuronal activities with TTX while under GlyR blockade were comparable to those of cSTR group (Fig. 7A & B). These results suggest that the mobile property of GlyR is independent of neuronal activity under blockade of GlyRs.

GlyR diffusion properties and synaptic localization depends on interactions with gephyrin, the scaffolding protein of inhibitory neurotransmitter receptors (Fritschy et al., 2008) and it is the indispensable element (Kirsch et al., 1993). Gephyrin interaction with GlyRβ loop is suggested to decrease lateral mobility of GlyRs (Schrader et al., 2004; Specht et al., 2011) by phosphorylation-dependent manner (Zita et al., 2007; Charrier et al., 2010). The present results show that the diffusion properties of GlyRs depends on their activation at gephyrin-expressing spots (Fig. 6D). Moreover, the effect of GlyR activation was suppressed by staurosporine (Fig. 9) indicating that activation-dependent decrease of synaptic GlyR mobility may be regulated by protein kinase-mediating gephyrin interaction. A recent study also showed that blockade of GlyRs decreases kinesin superfamily protein 5 (KIF5)-mediating intracellular gephyrin

transport (Maas et al., 2009). Although the comprehensive mechanism of GlyR-gephyrin interactions and trafficking are still not fully elusive, GlyR activation may play significant role for both gephyrin recruitment and trapping diffusive GlyRs at synapses.

At immature stages, the recovery of GlyR clustering after strychnine removal has been reported in cultured rat neurons (Lévi et al., 1998) and in vivo zebrafish (Yamanaka et al., 2013). These formations of synaptic GlyR clustering are considered to occur only at immature stages by glycine-induced depolarization (Kirsch & Betz, 1998). However, glycine-induced depolarization shifts to hyperpolarization (D-H shift) with increasing expression of KCC2 (Ben-Ari et al, 2007). In addition, another study reported that the prolonged GABA-induced depolarization period by chronic treatment of $GABA_A$ receptor inhibitor (Ganguly et al., 2001). However, the present result from gramicidin-perforated recording indicates that glycinergic inputs do not induce depolarizing but hyperpolarizing responses in the present study (after 14 div). This observation is consistent with acutely isolated neurons from the ventral tegmental area (Ye, 2000). Moreover, E_{gly} is not influenced by chronic treatment of strychnine (Fig. 12). Thus, this is a novel report that the activation-dependent GlyR formation at synapse in mature neurons. The detailed molecular mechanism is still under the cover, but the previously proposed mechanism of glycine-induced depolarization (Kirsch and Betz, 1998) is insufficient in mature neurons. Since GlyR activation induces its

conformational changes in both α1 and β subunits of GlyRα1β heteromer (Lynch, 2004), the modulation of gephyrin and GlyR interactions might be also involved in the activation-dependent GlyR localization.

Although GlyR activation restored its synaptic localization at matured stages, interestingly, the further strychnine treatment on the matured control group did not increase GlyR diffusion (Fig. 8B & C). The present observation seems opposite of the previous report which showed decreasing previously clustered GlyRs by later application of strychnine (Yamanaka et al., 2013). However, the study also reported that the effect of later application of strychnine was decreased with animal development (Yamanaka et al., 2013). Therefore, the activation of GlyR may be important for the formation but not for maintenance of synaptic clusters in mature neurons.

Overall, the present results support the previous observations demonstrating the GlyRα1 increase (Friauf et al., 1997; Piechotta et al., 2001) corresponding to increased presynaptic glycine release (Nabekura et al., 2004) at matured neuronal stage in vivo. The present results illustrate the molecular dynamics underlying the formation of glycinergic synapses. GlyRs activation by presynaptically released glycine decreases their lateral diffusion at the postsynaptic membrane. Thus, the relative amount of GlyRs stays longer duration and accumulates at synapses (Fig. 14A). Furthermore, the modulations of GlyR spatial dynamics affect postsynaptic response of glycinergic transmission, and this is consistent with developmental increase of synaptic GlyRs

37

(Singer & Berger, 1999). In the previous studies, the glycinergic synapse formation has been considered to be occurred at immature stage, but the present study suggests that activation-dependent glycinergic synapse formation is induced at matured stages. The rapid formation rather than maintenance of glycinergic synapses may be responsible for the functional role of rapid adaptation in the matured neural system.

References

Alvarez, F.J., Fyffe, R.E. (2007). The continuing case for the Renshaw cell. *J Physiol*. 584, 31-45.

Ashby, M. C., Ibaraki, K., & Henley, J. M. (2004). It's green outside: tracking cell surface proteins with pH-sensitive GFP. *Trends Neurosci*. 27, 257–261.

Bannai, H., Lévi, S., Schweizer, C., Dahan, M., & Triller, A. (2006). Imaging the lateral diffusion of membrane molecules with quantum dots. *Nat protoc*. 1, 2628–2634.

Bannai, H., Lévi, S., Schweizer, C., Inoue, T., Launey, T., Racine, V., Sibarita, J.B., Mikoshiba, K., & Triller, A. (2009). Activity-dependent tuning of inhibitory neurotransmission based on GABAAR diffusion dynamics. *Neuron*. 62, 670–682.

Ben-Ari, Y. (2002). Excitatory actions of GABA during development: the nature of the nurture. *Nat Rev Neurosci*. 3, 728–739.

Ben-Ari, Y., Gaiarsa, J.L., Tyzio, R., & Khazipov, R. (2007). GABA: a pioneer transmitter that excites immature neurons and generates primitive oscillations. *Physiol Rev*. 87, 1215–1284.

Bonneau, S., Dahan, M., & Cohen, LD. (2005). Single quantum dot tracking based on perceptual grouping using minimal paths in a spatiotemporal volume. *IEEE Trans Image Process.* 14, 1384–1395.

Borgdorff, A.J., & Choquet, D. (2002). Regulation of AMPA receptor lateral movements.

Nature. 417, 649–653.

Charrier, C., Machado, P., Tweedie-Cullen, R. Y., Rutishauser, D., Mansuy, I. M., & Triller, A. (2010). A crosstalk between β1 and β3 integrins controls glycine receptor and gephyrin trafficking at synapses. Nat Neurosci. 13, 1388–1395.

Dahan, M., Lévi, S., Luccardini, C., Rostaing, P., Riveau, B., & Triller, A. (2003). Diffusion dynamics of glycine receptors revealed by single-quantum dot tracking. *Science*. 302, 442–445.

Dutertre, S., Becker, C., & Betz, H. (2012). Inhibitory glycine receptors: an update. *J Biol Chem*. 287, 40216–40223.

Ebihara, S., Shirato, K., Harata, N., & Akaike, N. (1995). Gramicidin-perforated patch recording: GABA response in mammalian neurones with intact intracellular chloride. *J Physiol*. 1995. 484, 77–86.

Friauf, E., Hammerschmidt, B., & Kirsch, J. (1997). Development of adult-type inhibitory glycine receptors in the central auditory system of rats. *J Comp Neurol*, 385, 117–134.

Fritschy, J., Harvey, R., & Schwarz, G. (2008). Gephyrin: where do we stand, where do we go? *Trends Neurosci*. 31, 257–264.

Gaffield, MA., & Betz, WJ., (2007). Imaging synaptic vesicle exocytosis and endocytosis with FM dyes. *Nat Protoc*. 1, 2916–2921.

Ganguly, K., Schinder, A.F., Wong, S.T., & Poo, M. (2001). GABA itself promotes the

developmental switch of neuronal GABAergic responses from excitation to inhibition. *Cell*. 105, 521–532.

Hildick, K. L., González-González, I. M., Jaskolski, F., & Henley, J. M. (2012). Lateral diffusion and exocytosis of membrane proteins in cultured neurons assessed using fluorescence recovery and fluorescence-loss photobleaching. *J Vis Exp*. 60, 1–9.

Kakazu, Y., Akaike, N., Komiyama, S., & Nabekura, J. (1999). Regulation of intracellular chloride by cotransporters in developing lateral superior olive neurons. *J Neurosci*. 19, 2843–2851.

Kirsch, J., & Betz, H. (1998). Glycine-receptor activation is required for receptor clustering in spinal neurons. *Nature*. 392, 717–720.

Kirsch, J., Wolters, I., Triller, A., & Betz, H. (1993). Gephyrin antisense oligonucleotides prevent glycine receptor clustering in spinal neurons. *Nature*. 366, 745–748.

Kuriu, T., Yanagawa, Y., & Konishi, S. (2011). Activity-dependent coordinated mobility of hippocampal inhibitory synapses visualized with presynaptic and postsynaptic tagged-molecular markers. *Mol Cell Neurosci*. 49, 184–195.

Lévi , S., Vannier, C., & Triller, A. (1998). Strychnine-sensitive stabilization of postsynaptic glycine receptor clusters. *J Cell Sci*. 111, 335–345.

Lévi , S., Schweizer, C., Bannai, H., Pascual, O., Charrier, C., & Triller, A. (2008). Homeostatic regulation of synaptic GlyR numbers driven by lateral diffusion. *Neuron*. 59, 261–273.

Lynch, J. W. (2004). Molecular structure and function of the glycine receptor chloride channel. *Physiol Rev*. 84, 1051–1095.

Lynch, J. W., & Callister, R. J. (2006). Glycine receptors: a new therapeutic target in pain pathways. C*urr Opin Investig Drugs*. 7, 48–53.

Maas, C., Belgardt, D., Lee, H. K., Heisler, F. F., Lappe-Siefke, C., Magiera, M. M., van Dijk, J., Hausrat, T. J., Janke, C., Kneussel, M. (2009). Synaptic activation modifies microtubules underlying transport of postsynaptic cargo. *Proc Natl Acad Sci*. 106, 8731–8736.

McDearmid, J. R., Liao, M., Drapeau, P. (2006). Glycine receptors regulate interneuron differentiation during spinal network development. *Proc Natl Acad Sci*. 103, 9679–9684.

Meyer, G., Kirsch, J., Betz, H., & Langosch, D. (1995). Identification of a gephyrin binding motif on the glycine receptor beta subunit. *Neuron*. 15, 563–572.

Meier, J., Vannier, C., Sergé, A., Triller, A., & Choquet, D. (2001). Fast and reversible trapping of surface glycine receptors by gephyrin. *Nat Neurosci*. 3, 253–260.

Miesenböck, G., De Angelis, D. A., & Rothman, J. E. (1998). Visualizing secretion and synaptic transmission with pH-sensitive green fluorescent proteins. *Nature*. 394,

192–195.

Murase, K., Ryu, P. D., & Randić, M. (1989). Excitatory and inhibitory amino acids and peptide-induced responses in acutely isolated rat spinal dorsal horn neurons. *Neurosci Lett*. 103, 56–63.

Nabekura, J., Katsurabayashi, S., Kakazu, Y., Shibata, S., Matsubara, A., Jinno, S., Mizoguchi, Y., Sasaki, A., Ishibashi, H. (2004). Developmental switch from GABA to glycine release in single central synaptic terminals. *Nat Neurosci*. 7, 17–23.

Piechotta, K., Weth, F., Harvey, R. J., & Friauf, E. (2001). Localization of rat glycine receptor alpha1 and alpha2 subunit transcripts in the developing auditory brainstem. The Journal of comparative neurology, 438(3), 336–52.

Rannals, M. D., & Kapur, J. (2011). Homeostatic Strengthening of Inhibitory Synapses Is Mediated by the Accumulation of GABAA Receptors. *J Neurosci*.31, 17701–17712.

Reits, E. A., & Neefjes, J. J. (2001). From fixed to FRAP: measuring protein mobility and activity in living cells. *Nat Cell Biol*. 3, E145–147.

Rasmussen, H., Rasmussen, T., Triller, A., & Vannier, C. (2002). Strychnine-blocked glycine receptor is removed from synapses by a shift in insertion/degradation equilibrium. *Mol Cell Neurosci*, 19, 201–215.

Sanes, D. H., Malone, B. J., & Semple, M. N. (1998). Role of synaptic inhibition in processing of dynamic binaural level stimuli. *J Neurosci*. 18, 794–803.

Sankaranarayanan, S., & Ryan, T.A. (2001). Calcium accelerates endocytosis of vSNAREs at hippocampal synapses. *Nat Neurosci*. 4, 129–136.

Schrader, N., Kim, E. Y., Winking, J., Paulukat, J., Schindelin, H., & Schwarz, G. (2004). Biochemical characterization of the high affinity binding between the glycine receptor and gephyrin. *J Biol Chem*. 279, 18733–18741.

Singer, J. H., & Berger, A. J. (1999). Contribution of single-channel properties to the time course and amplitude variance of quantal glycine currents recorded in rat motoneurons. *J Neurophysiol*. 81, 1608–1616.

Soumpasis, DM. (1983). Theoretical analysis of fluorescence photobleaching recovery experiments. *Biophys J*. 41, 95–97.

Specht, CG., Grünewald, N., Pascual, O., Rostgaard, N., Schwarz, G., & Triller, A. (2011). Regulation of glycine receptor diffusion properties and gephyrin interactions by protein kinase C. *EMBO J*, 1–12.

Vaello, ML., Ruiz-Gómez, A., Lerma, J., & Mayor F Jr. (1994). Modulation of inhibitory glycine receptors by phosphorylation by protein kinase C and cAMP-dependent protein kinase. *J Biol Chem*. 269, 2002–2008.

Waataja, J. J., Kim, H. J., Roloff, A. M., & Thayer, S. A. (2008). Excitotoxic loss of

post-synaptic sites is distinct temporally and mechanistically from neuronal death. *J Neurochem*. 104, 364–375.

Wang, Y., Kakizaki, T., Sakagami, H., Saito, K., Ebihara, S., Kato, M., Hirabayashi, M., Saito, Y., Furuya, N., & Yanagawa, Y. (2009). Fluorescent labeling of both GABAergic and glycinergic neurons in vesicular GABA transporter (VGAT)-venus transgenic mouse. *Neuroscience*. 164, 1031–1043.

Wässle, H., Heinze, L., Ivanova, E., Majumdar, S., Weiss, J., Harvey, R. J., Haverkamp, S. (2009). Glycinergic transmission in the Mammalian retina. *Front Mol Neurosci*. 2, 1–12.

Yamanaka, I., Miki, M., Asakawa, K., Kawakami, K., Oda, Y., & Hirata, H. (2013). Glycinergic transmission and postsynaptic activation of CaMKII are required for glycine receptor clustering in vivo. *Genes Cells*. 18,211–224.

Ye, j. (2000). Physiology and pharmacology of native glycine receptors in developing rat ventral tegmental area neurons. *Brain Res*. 862, 74–82.

Zita, M. M., Marchionni, I., Bottos, E., Righi, M., Del Sal, G., Cherubini, E., & Zacchi, P. (2007). Post-phosphorylation prolyl isomerisation of gephyrin represents a mechanism to modulate glycine receptors function. *EMBO J*. 26, 1761–71.

Figure Legends and Figures

Figure 1. Decreased synaptic GlyRα1 localization under chronic strychnine treatment

(A) Schematic diagrams of three main groups used in the present study. Control group is maintained without strychnine. Chronic strychnine-applied group (cSTR) had been maintained 1 μM strychnine since the first day in vitro. WASH group was also treated 1 μM strychnine from the first day in vitro, but exchanged to the normal medium-lacking strychnine since one hour prior to each experiment.

(B-D) Representative images of double immunostaining of VIAAT (VGAT) and glycine receptor α1 (GlyRα1) in cultured rat spinal cord neurons (30-39 div). (B), (C), (D) represents control, cSTR, and WASH groups, respectively.

(E) Colocalization index of GlyR α1 at inhibitory synapses. Scale bar= 10 μm. * $p <$ 0.05, ** $p<0.005$.

A

14-42 DIV incubation   Experiment

Control
cSTR
WASH

STR removal
1h before experiment

Control   **cSTR**   **WASH**

Merged   B1   C1   D1

10 μM

VIAAT   B2   C2   D2

GlyRα1   B3   C3   D3

E

merged GlyR / total GlyR

**   **   ** **

0.6
0.4
0.2
0

Control   cSTR   WASH
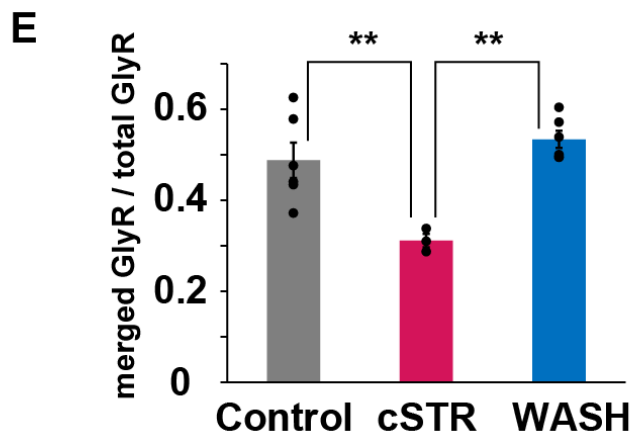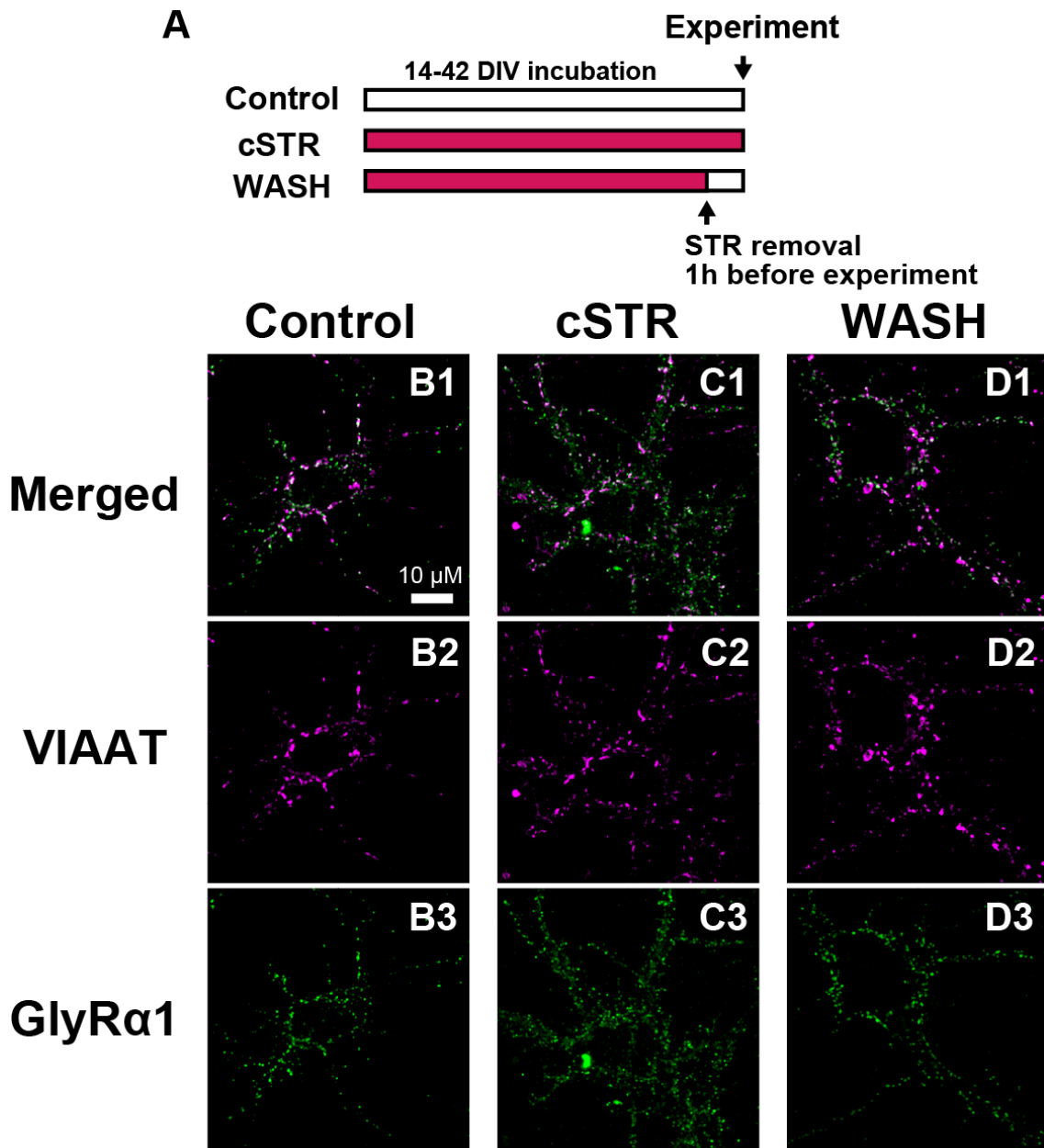
Figure 1

Figure 2. Immunoblotting analysis of GlyR on cell surface and lysates of cells

(A) In control, chronic strychnine treatment (cSTR) and one hour after removal of chronically applied strychnine (WASH), neurons were surface-biotinylated with the sulfo-NHS-SS biotin. Biotinylated membrane proteins (surface) were isolated from detergent soluble fractions (total) with immobilized NeutrAvidin and were immunoblotted with the antibodies against GlyR α1–4 and β subunits and β actin.

(B) Quantification of total and surface-expressed GlyRα1-4 in control, chronic strychnine treatment (cSTR) and one hour after removal of chronically applied strychnine (WASH). (n=1)

A

Total

| | Control | cSTR | WASH |

GlyRα1-4

ß-actin

Surface

| | Control | cSTR | WASH |

GlyRα1-4
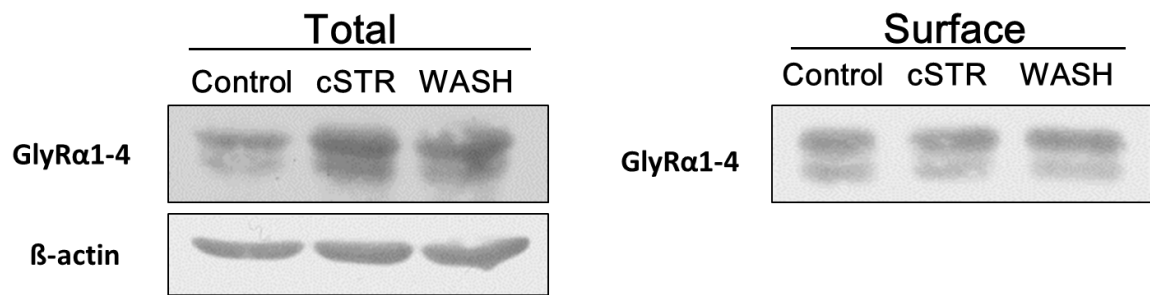
B
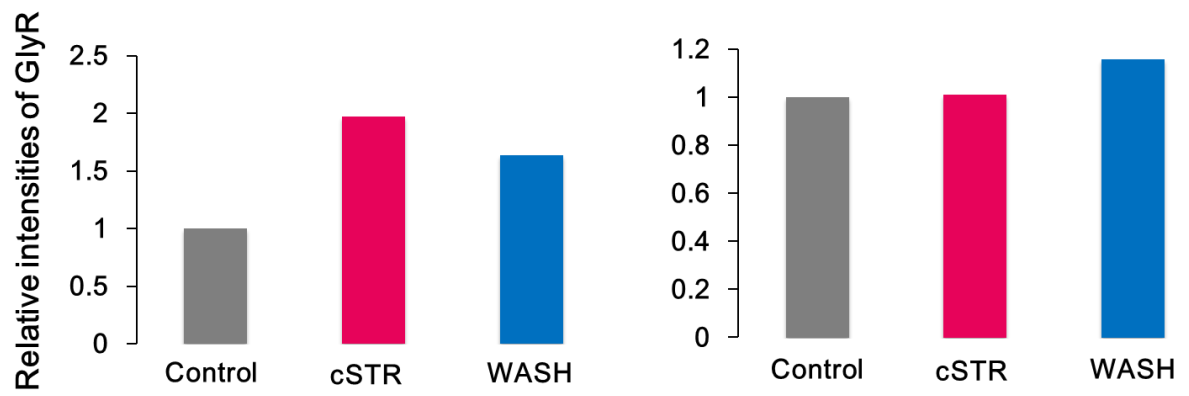
Figure 2

Figure 3. Selective visualization of cell surface GlyRα1

(A) Schematic picture of superecliptic pHluorin (SEP), pH-sensitive GFP,-tagged GlyRα1 construct used for FRAP (and FRAP-FLIP) experiment.

(B) pCAG-SEP-GlyRα1expressed neurites in cultured spinal cord neuron. Acidification of extracellular solution (pH 5.4) successively abolished fluorescence intensity of SEP, and the fluorescence was restored within 1 minute after returned to pH 7.4 (97.4 % fluorescence intensity was recovered within 1 minutes in this example).

(C) Schematic illustration of pCAG-SEP-GlyR trafficking at the cytoplasmic membrane.

A

| CAG | signal peptide | SEP | mGlyRα1 |

B

pH 7.4 ➡ pH 5.4 ➡ pH 7.4 (1min)

2.5 µm

C

SEP-tagged GlyR

pH 7.4

Lateral diffusion

Cytoplasmic membrane

Endocytosis

Exocytosis
(membrane insertion)

pH 5.5

Secretory vesicle
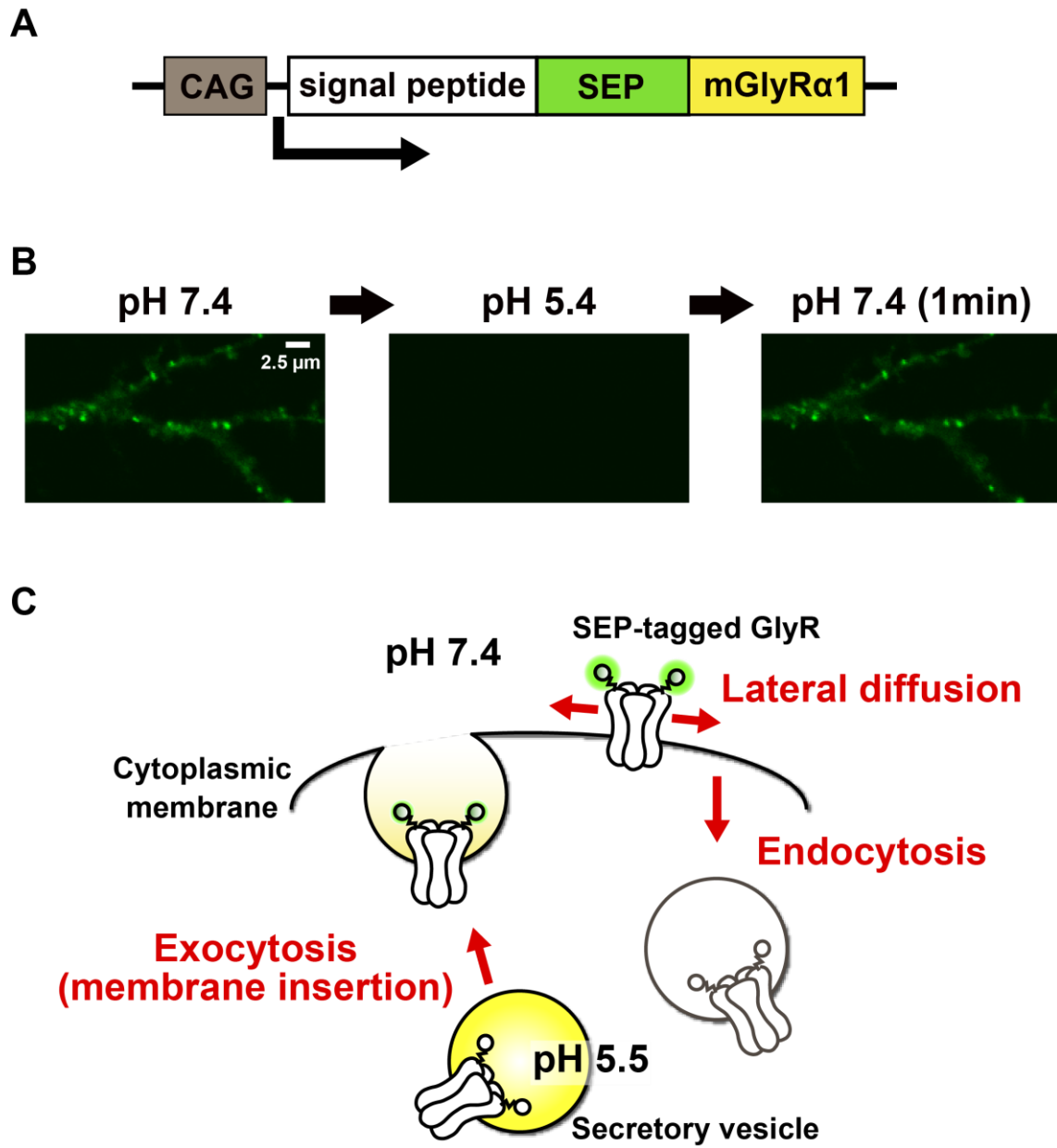
Figure 3

Figure 4. Rapid fluorescence recovery under blockade of GlyR

(A) Representative examples of fluorescence recovery after photobleaching (FRAP) experiment (upper: control, middle: chronic strychnine treatment, lower: one hour after chronic strychnine removal). Neural processes expressing SEP-GlyRα1 were photobleached at 3 x 5 μm ROI (red squares), and measured the fluorescence intensities after photobleaching. The fluorescence intensity is shown as ratiometric image. Scale bar represents 2 μm.

(B) Average normalized fluorescence intensities in each group (mean ± SEM). Chronic strychnine treatment groups (cSTR; magenta, n=7) showed higher fluorescence recovery than control (black, n=7) and WASH (light blue, n=5) groups. Even with brefeldin A, an exocytosis inhibitor, fluorescence recovery rate was higher under the chronic strychnine treatment (green, n=5).

 (C) Average normalized intensities from last 3 frames (248-257 seconds after bleaching: yellow highlighted time points in panel B) in control (n=7), cSTR (n=7), WASH (n=5) and cSTR+BFA (n=5) groups (mean ± SEM). ***$p < 0.001$; n.s., no significance.

A

	Prebleach	1st frame postbleach	Last frame
Control			
cSTR			
WASH			

2 μm

B

Control
cSTR
WASH
cSTR+BFA

Normalized intensity

1.0
0.8
0.6
0.4
0.2
0

-13 20 49 78 107 136 165 193 222 251

(sec)

C

Normalized intensity

0.5
0.4
0.3
0.2
0.1
0

n.s.
***
***

Control cSTR WASH cSTR+BFA

Figure 4

53
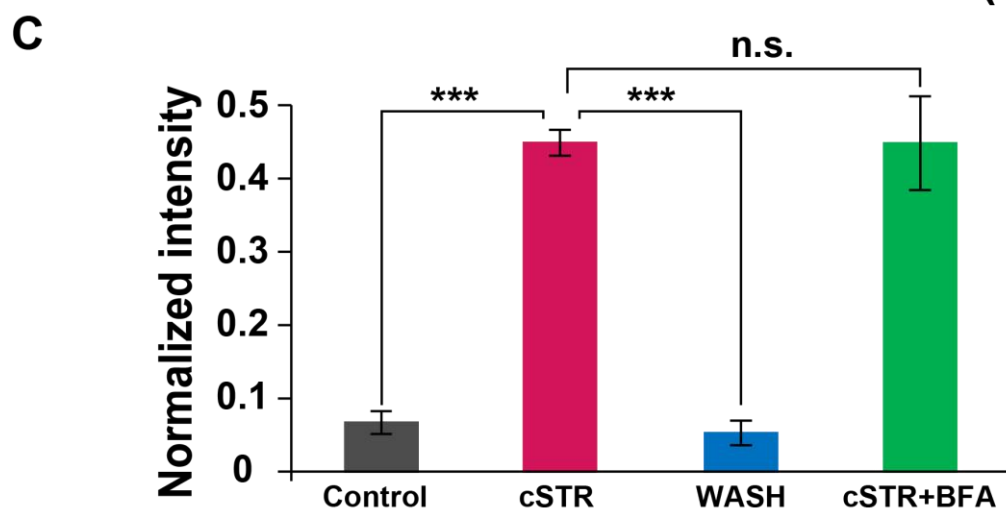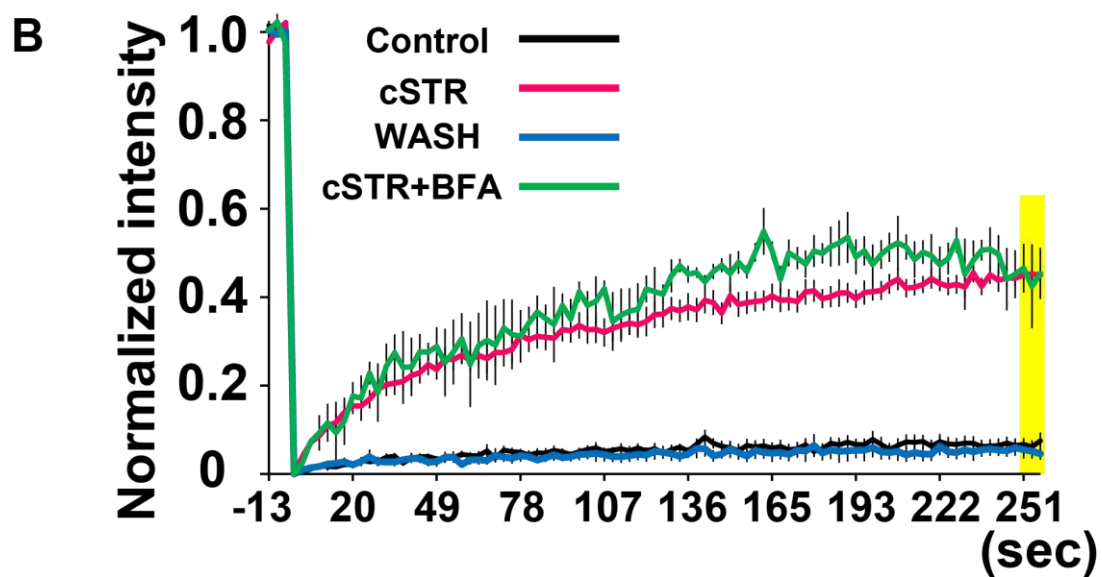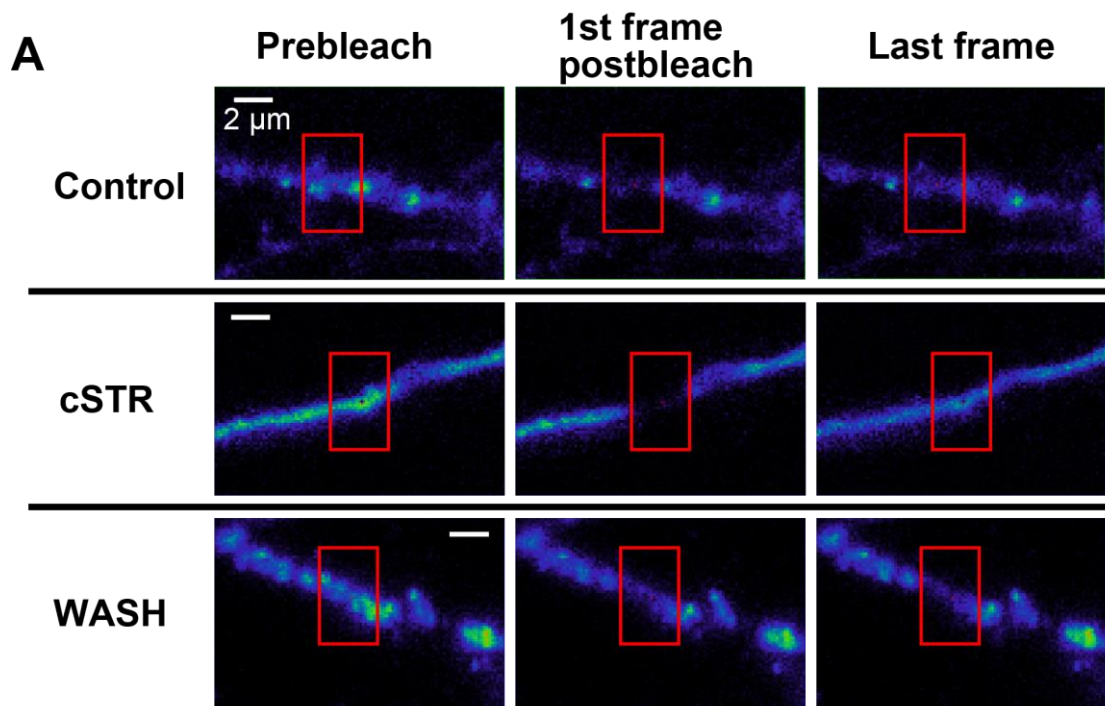
Figure 5. FRAP-FLIP protocol for distinguishing exocytosis and lateral diffusion

(A) Schematic illustration of FRAP-FLIP protocol. Blue area represents initial

bleaching region. Fluorescence loss in photobleaching (FLIP) was performed in the

both sides of the initial belching region. Continuous bleaching prevents fluorescence

recovery by laterally diffusing SEP-GlyRs. Fluorescence intensity was measured at

FRAP ROI (red area) which is same size in both FRAP-only and FRAP-FLIP protocols

(3 x 5 μm). FRAP-FLIP protocol doesn't change diffusion properties, but recovered

fluorescence intensity can be attributed to newly exocytosed SEP-GlyRs.

(B) Average normalized fluorescence intensities in each group (mean ± SEM).   The

solid lines and dashed lines represent FRAP-only (shown in Fig. 4B & C) and

FRAP-FLIP protocols, respectively.

 (C) Average normalized fluorescence intensities from last 3 frames (248-257 seconds

after bleaching: yellow highlighted time points in panel B) in control (n=7), cSTR (n=7),

WASH (n=5) groups (mean ± SEM). Filled bars represent FRAP-Only and striped bars

represent FRAP-FLIP protocols. ***$p < 0.001$; n.s., no significance.

A

FLIP ROI
(continuous bleaching)

Exocytosis

Lateral diffusion

FRAP ROI
(for measurement)

Initial bleaching region

B

FRAP +FLIP

Control
cSTR
WASH

Normalized intensity

1.0
0.8
0.6
0.4
0.2
0

-13 20 49 78 107 136 165 193 222 251
(sec)

C

Normalized intensity

0.5
0.4
0.3
0.2
0.1
0

n.s.   ***   n.s.

FRAP +FLIP | FRAP +FLIP | FRAP +FLIP
Control | cSTR | WASH
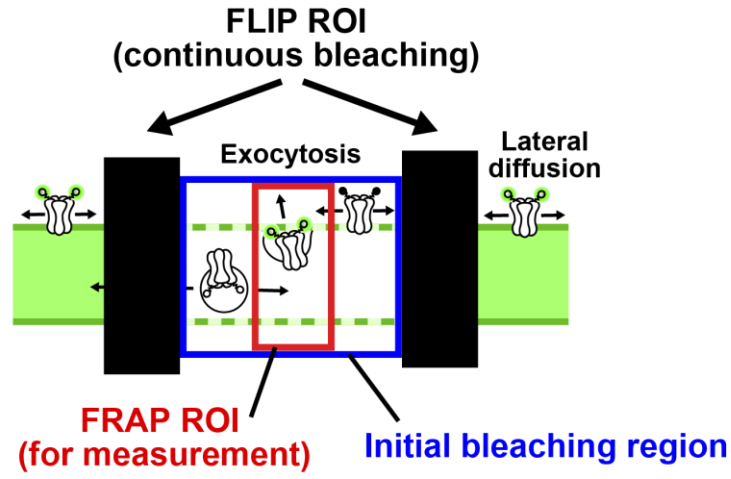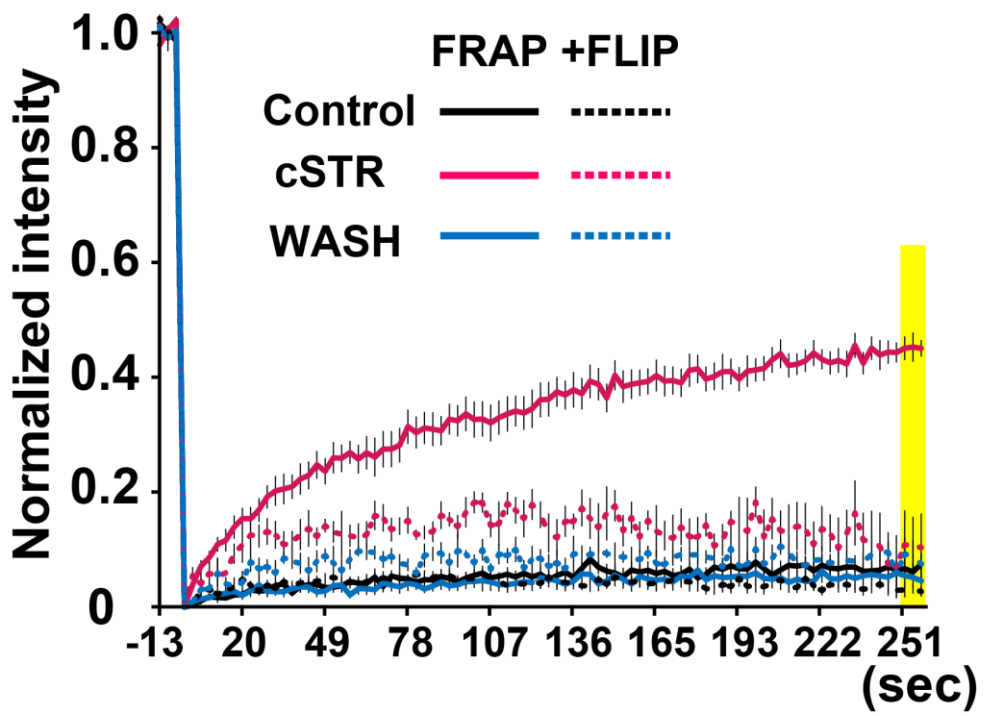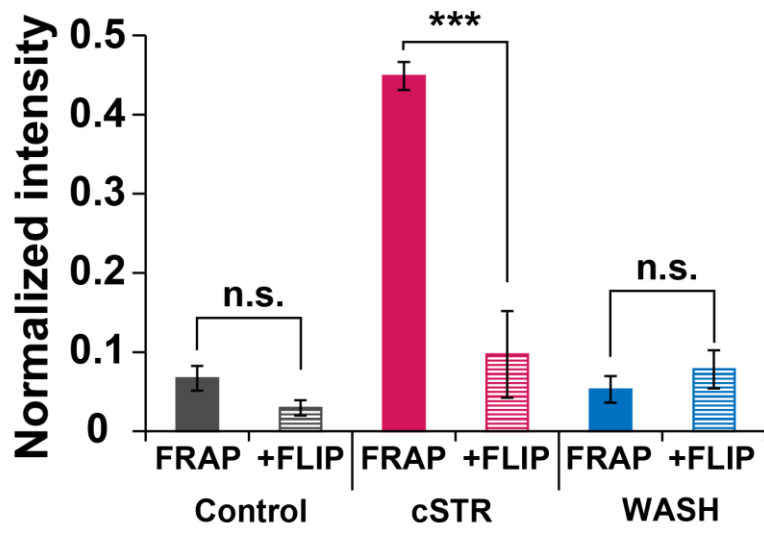
Figure 5

Figure 6. Focal FRAP at synapse and extrasynapse

(A) Construct of mCherry-tagged gephyrin, a postsynaptic scaffolding protein of glycine receptors used as a marker of postsynaptic structure.

(B) Representative image of process of cultured neuron expressing SEP-GlyRα1 (upper panel) and mCherry-gephyrin (lower panel).Measurements of fluorescence recovery after photobleaching (FRAP) were performed using focal ROIs (1 µm diameter circle) at mCherry-gephyrin-expressed (red circle) and absent (yellow circle) spots. NOTE: In the most of mCherry-expressed cells, the signals showed punctate structures. Higher fluorescence intensities of SEP-GlyRα1 were observed at mCherry signals especially in control group, but this was varied in each neuron even on the same cover slip.

(C) Average normalized fluorescence intensities at mCherry-gephyrin expressed (solid line) and absent (dashed line) spots (mean ± SEM).

(D) Average normalized fluorescence intensities at mCherry-gephyrin expressed spots in control (black, n=14), cSTR (magenta, n=8), WASH (light blue, n=15) groups (mean ± SEM).

(E) Average normalized fluorescence intensities from last 3 frames (258-267 seconds

after bleaching: yellow highlighted time points in panels C and D) in control (black,

n=14), cSTR (magenta, n=8), WASH (light blue, n=15) groups (mean ± SEM).Filled

and striped bars represent FRAP ROI at mCherry expressed and absent spots,

respectively. ***$p < 0.001$. n.s., no significance.
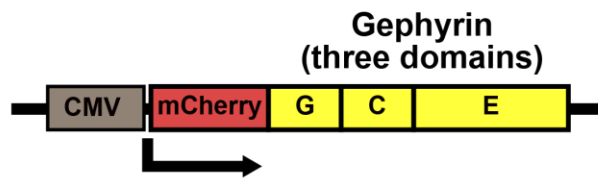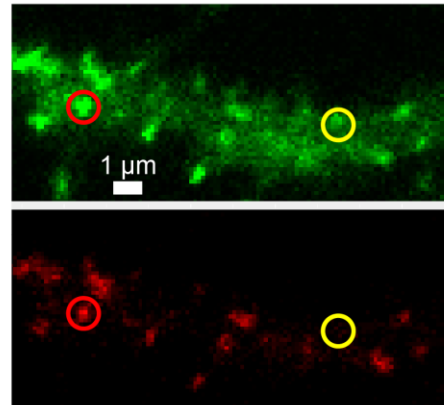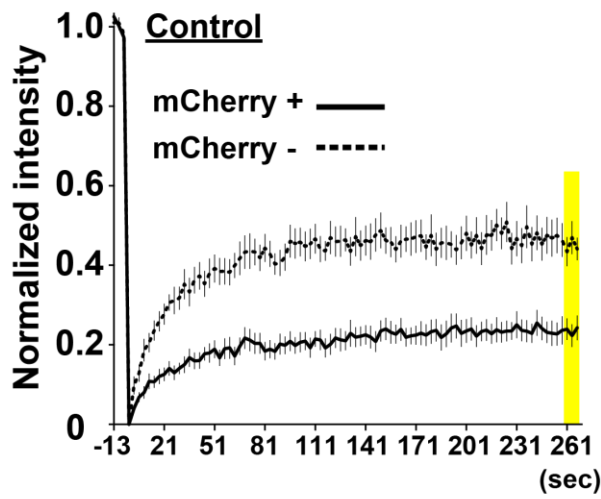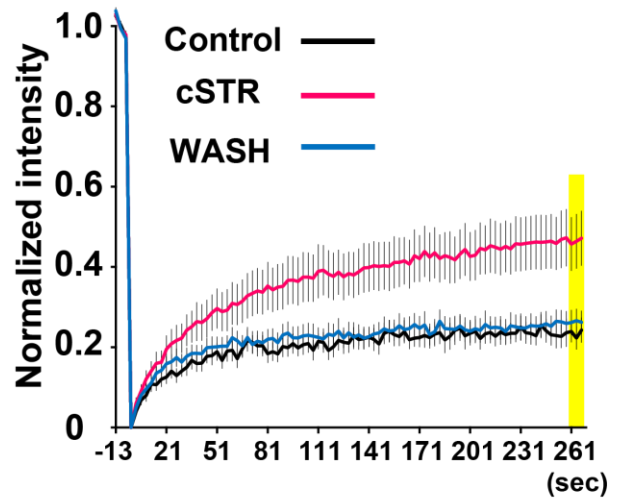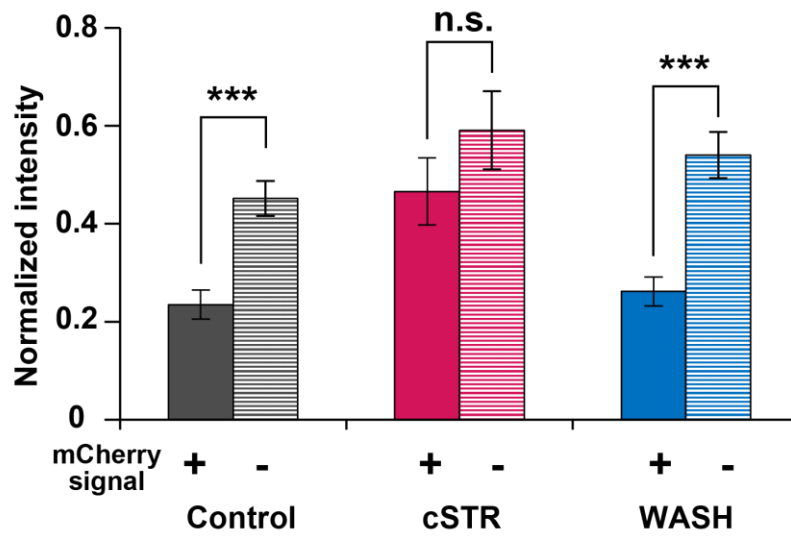
Figure 6

Figure 7. Activity independent mobility of GlyRα1 at synapses

(A) Average normalized fluorescence intensities under the chronic applications of TTX (blue), AP-V+CNQX (orange) in cSTR groups. cSTR (shown in Fig. 6D & E) is plotted as control of them (magenta) (mean ± SEM).

(B) Average normalized fluorescence intensities from last 3 frames (258-267 seconds after bleaching: yellow highlighted time points in panel A; mean ± SEM). n.s., no significance.

A
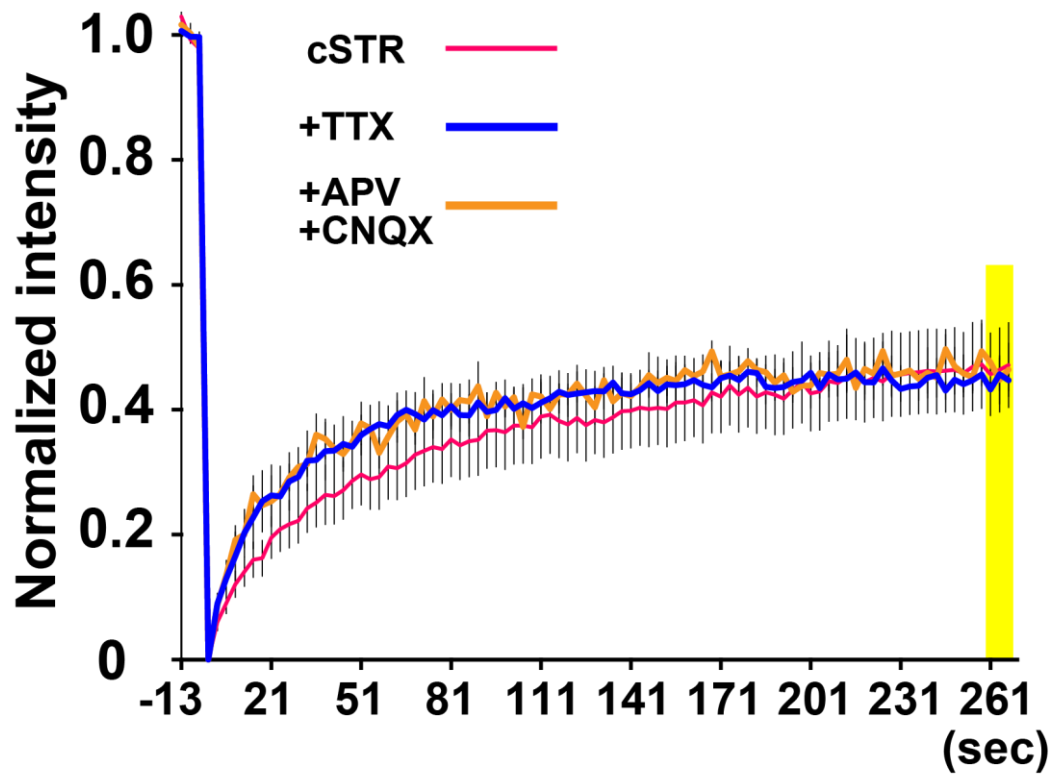
B
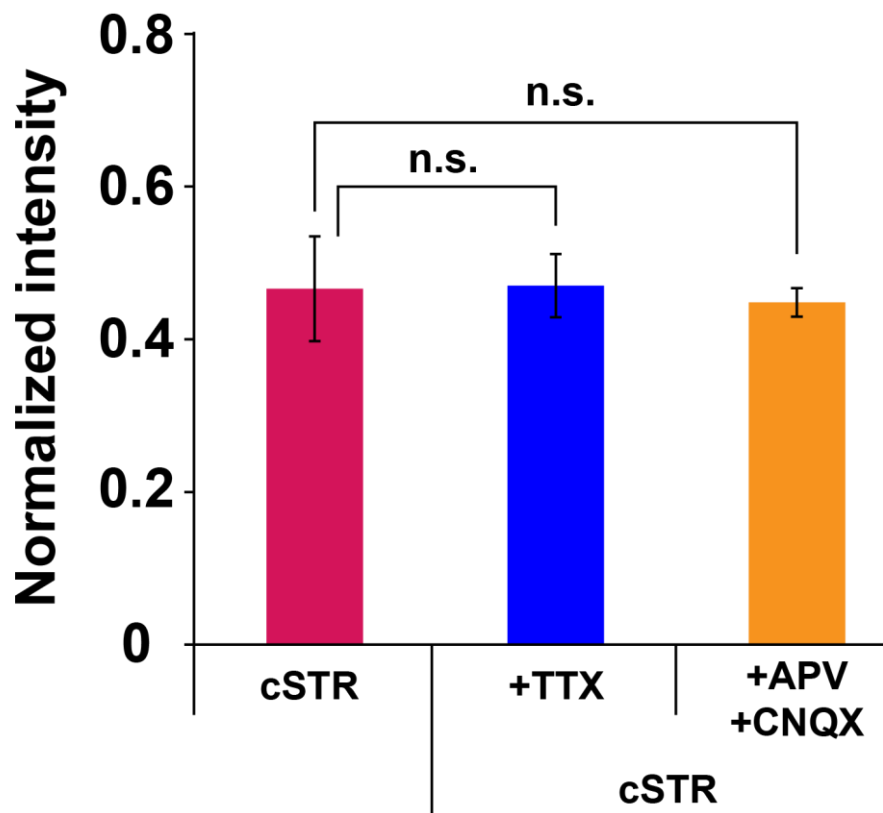
Figure 7

Figure 8. No effects of late applications of strychnine on the less mobile GlyRα

(A) Schematic diagrams of acute strychnine application protocol. Strychnine was applied to control group immediately, one hour, and 24 hours prior to experiments. Each imaging was performed under the presence of 1 μM strychnine.

(B) Average normalized fluorescence intensities under 1 μM strychnine applications acutely (STR 0h; green, n=5), prior to one hour (STR 1h; gray, n=9) and prior to 24 hours (STR 24h; orange, n=5) in control group (mean ± SEM). Control (without strychnine, black, shown in Fig. 6C, D & E) and chronic strychnine treatment (cSTR; magenta, shown in Fig. 6D) are plotted as control of them (mean ± SEM).

(C) Average normalized fluorescence intensities from last 3 frames (258-267 seconds after bleaching: yellow highlighted time points in panel A; mean ± SEM). n.s., no significance.

A

Experiment

14-42 DIV incubation

cSTR

Control

24h 1h 0h

STR application before experiment

B

cSTR
Control
+STR 0h
+STR 1h
+STR 24h

C

Control
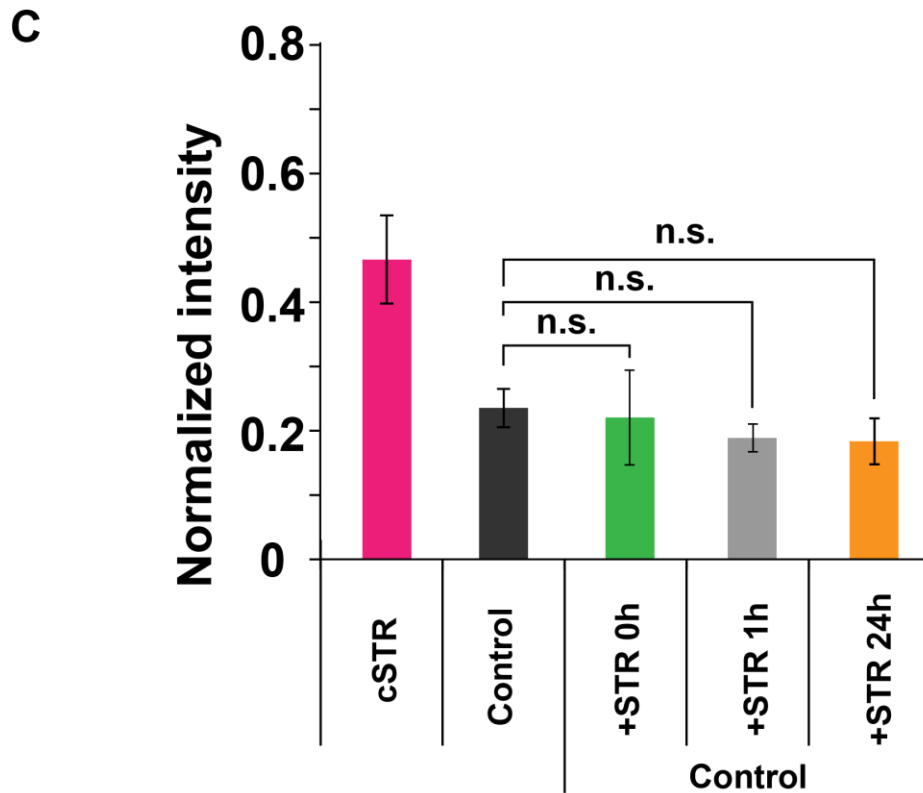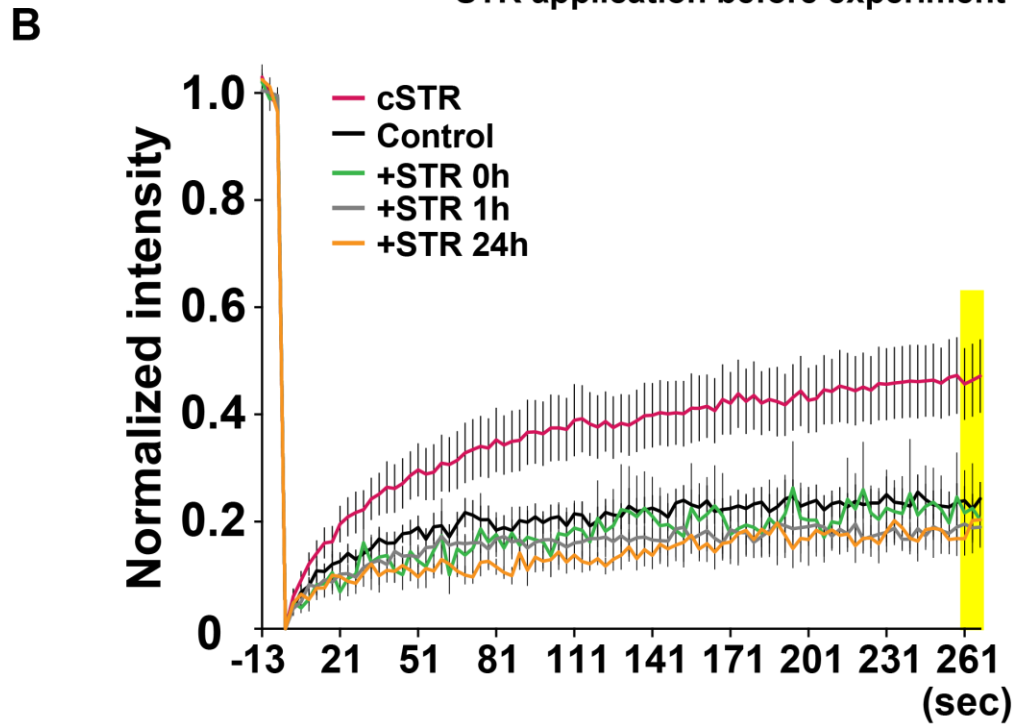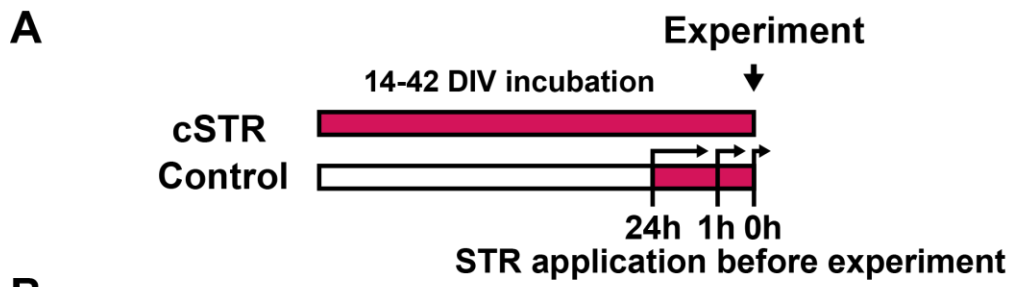
Figure 8

Figure 9. Effects of kinase inhibitors on activation-dependent GlyRα mobility

(A) Average normalized fluorescence intensities in the presence of kinase inhibitors or Ca^{2+} chelator in WASH group (mean ± SEM). Staurosporine (green, n=7), KN 62 (gray, n=7), Rp-cAMPs (orange, n=7), and BAPTA-AM (purple, n=5) were individually applied when chronically-applied strychnine (1 μM) was removed and incubated for one hour.   Control (black, shown in Fig. 6C & 6D) and cSTR (magenta, shown in Fig. 6D) and WASH (light blue, shown in Fig. 6D) groups are also plotted (mean ± SEM).

(B) Average normalized fluorescence intensities from last 3 frames (258-267 seconds after bleaching: yellow highlighted time points in panel A; mean ± SEM). *p < 0.05; n.s., no significance (compared with WASH group).
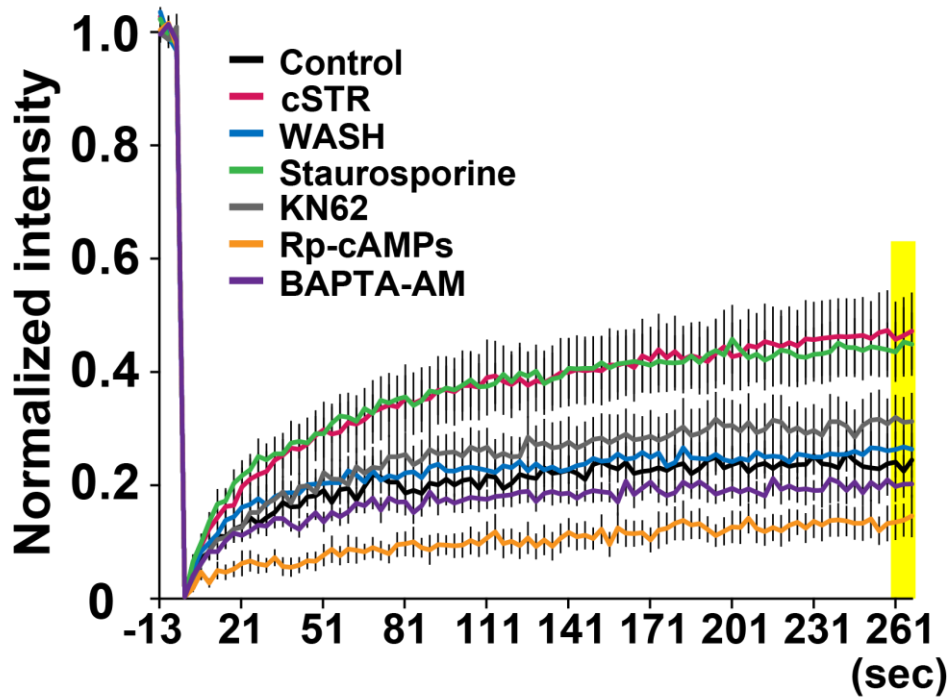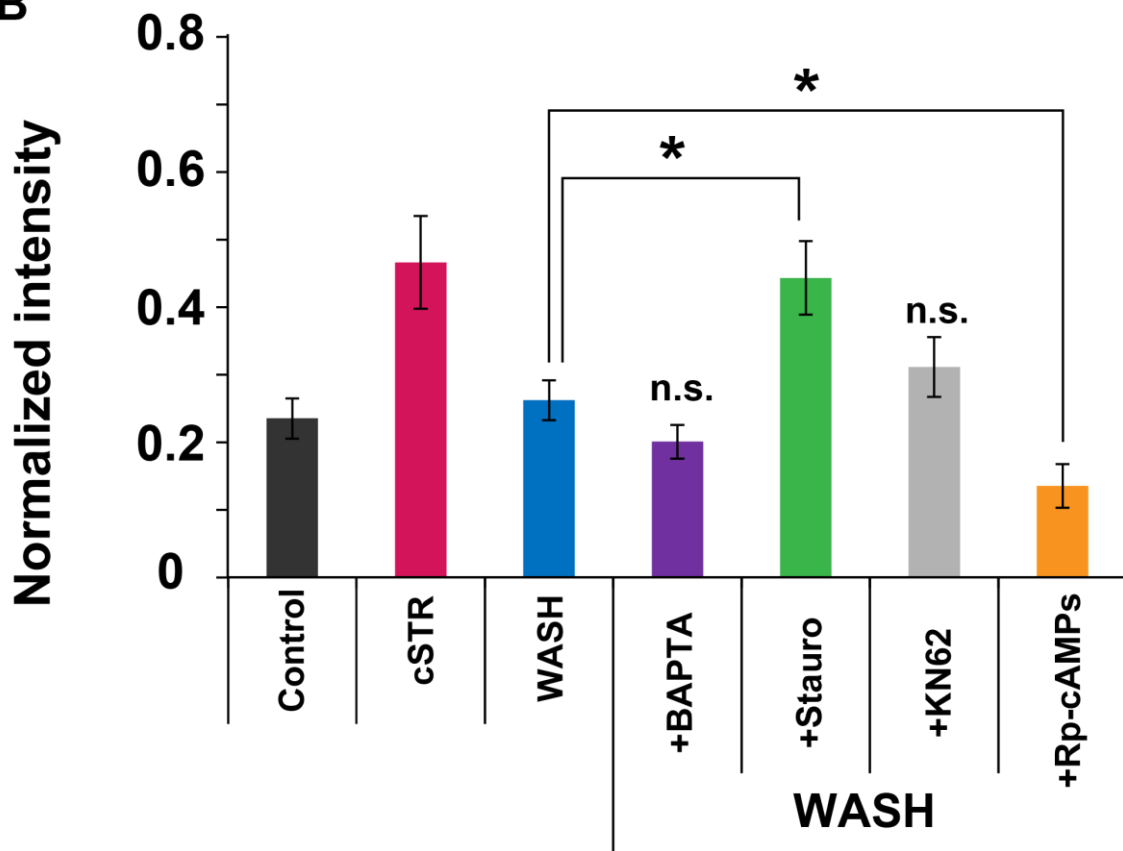
Figure 9

Figure 10. Single particle tracking of laterally diffusing GlyRs

(A) Representative example of quantum dot-labeled GlyR (QD-GlyR, red). QD-GlyR diffused along the neuronal process (green) and stayed at FM4-64-labeled synaptic region (blue).

(B) Cumulative histograms of activated QD-GlyRs (control group) classified by their diffusion coefficient (μm^2/sec) at synaptic (left) and extrasynaptic (right) regions (n=28). Scale bar, 1 μm.

(C) Superimposed image of QD-GlyR trajectories constructed from 30 seconds (300 frames) recordings in control (left) and cSTR (right) groups. Trajectories at synaptic (green) and extrasynaptic (blue) regions. Scale bars, 2 μm.

(D) Instantaneous diffusion coefficient (D_{inst}) of QD-GlyRs (shown in panel C) during 30 seconds recordings in control (left) and cSTR (right) groups. Upper lines (red) show their synaptic locations. In control groups, QD-GlyR showed relatively lower diffusion coefficient and stayed longer duration at synaptic region.

A

0 sec   2 sec   4 sec

1 µm

QD-GlyR
FM4-64
neurite

B

synapse

Number of QD-GlyRs

extrasynapse

Diffusion coefficient (µm²/s)

C

Control   cSTR

2 µm

synapse
extrasynapse

D

Control   cSTR

D_{inst} (µm²/s)

synaptic location

(sec)   (sec)
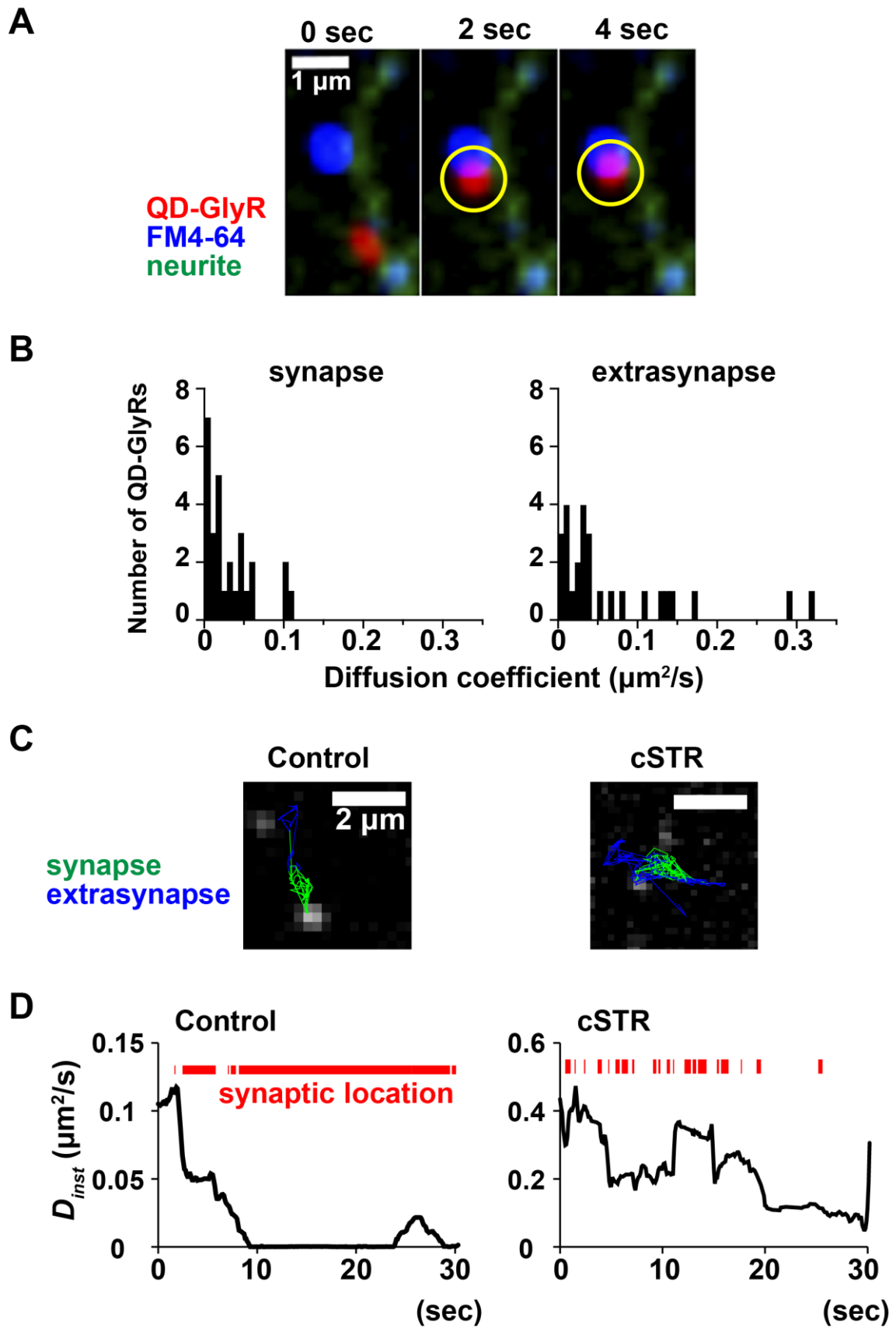
Figure 10

Figure 11. Changing diffusion properties of synaptic GlyR by its activation

(A) Median diffusion coefficients (black bar in each boxe) and interquartile ranges (each box) in control (black, n=28), cSTR (magenta, n=90) and WASH (light blue, n=14) groups.

(B) Cumulative histograms of QD-GlyRs dwell time at synapses. Relatively larger proportions of longer dwell time were seen in control (black, n=150) and WASH (blue, n=97), compared with cSTR (magenta, n=314) group.

(C) Average synaptic dwell time of QD-GlyR in control (black, n=150), cSTR (magenta, 314) and WASH (blue, n=97) groups (mean ± SEM). *p < 0.05, ***p < 0.001; n.s., no significance.
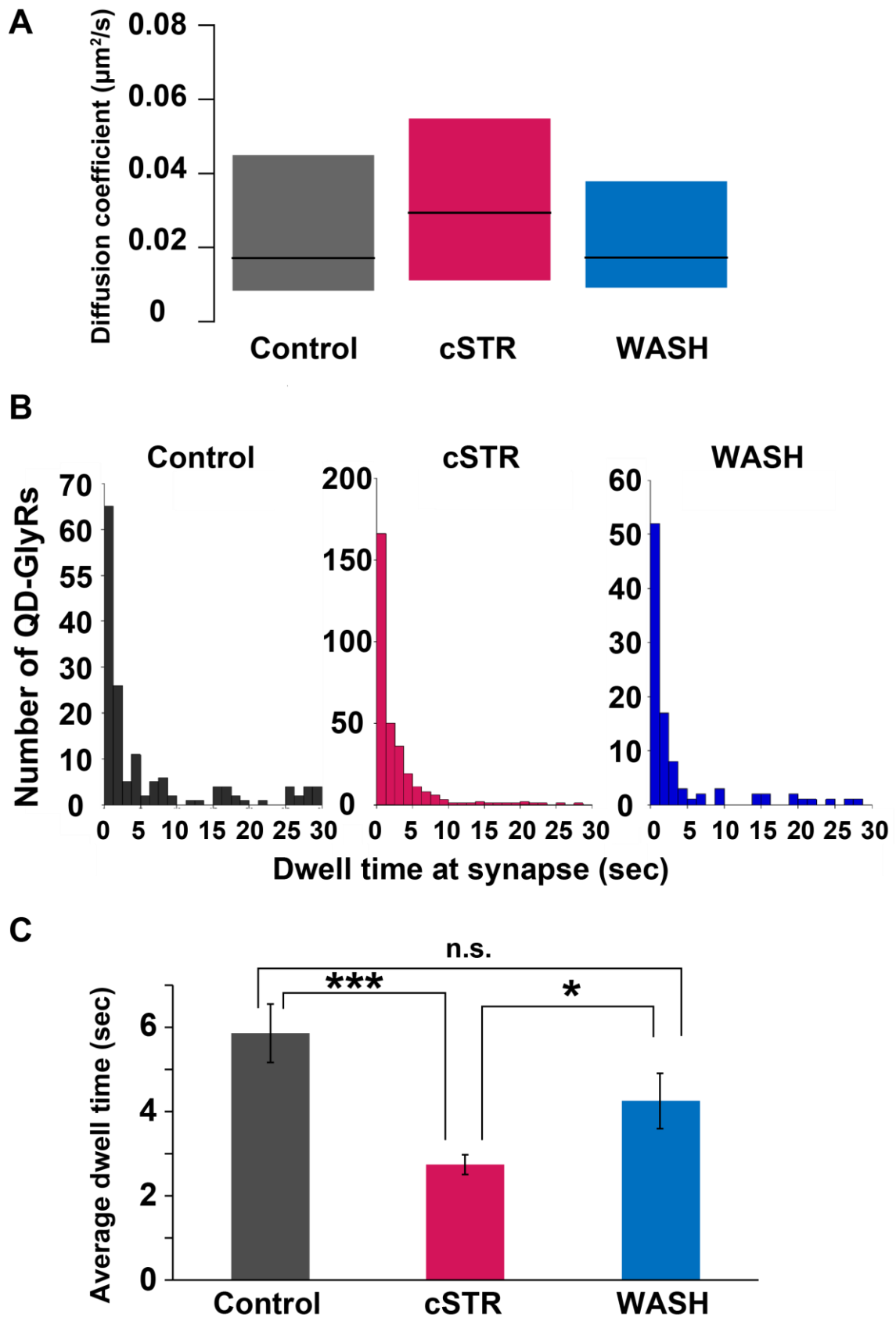
Figure 11

Figure 12. Reversal potentials of glycine-induced currents

(A) Representative traces of 100 μM glycine-induced currents (with ramp pulses from -110 to +40 mV for 1.6 seconds, right top). Arrowheads, a and b are examples of timing applying ramp pulses) of control and cSTR groups under the voltage-clamp configuration (V_H: -50 mV) of gramicidin-perforated patch recordings in the presence of TTX, CNQX, AP-V, SR95531.

(B) Average reversal potentials of 100 μM glycine-induced currents in control (n=6) and cSTR (n=5) groups (mean ± SEM).

A

Control

Gly 100 μM

cSTR

Gly 100 μM

+40 mV
-50 mV
-110 mV

50 pA

10 s

a   b

B

Control   cSTR

E_{gly} (mV)

-60

-70

-80

n.s.
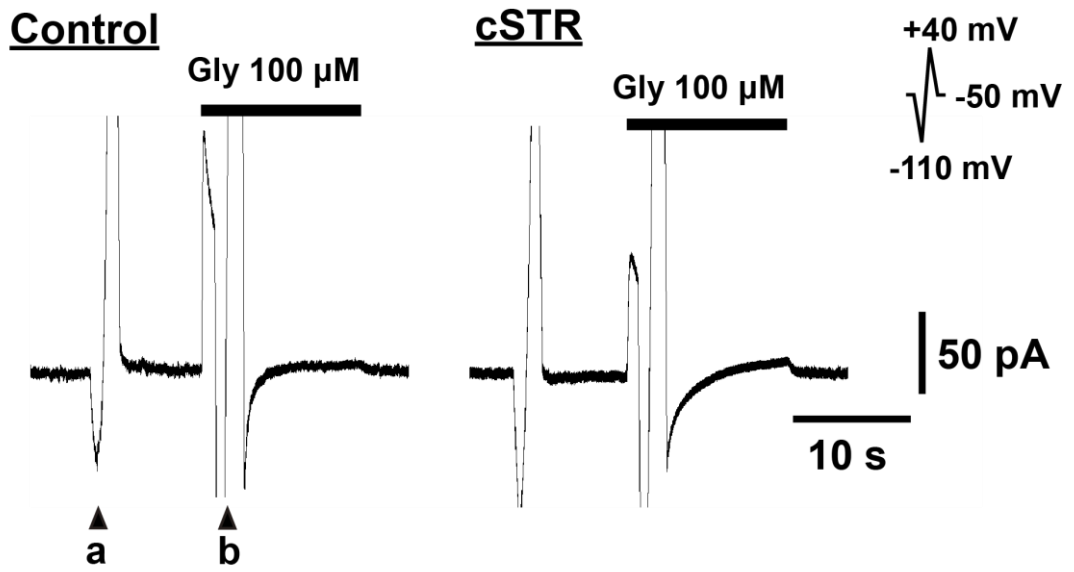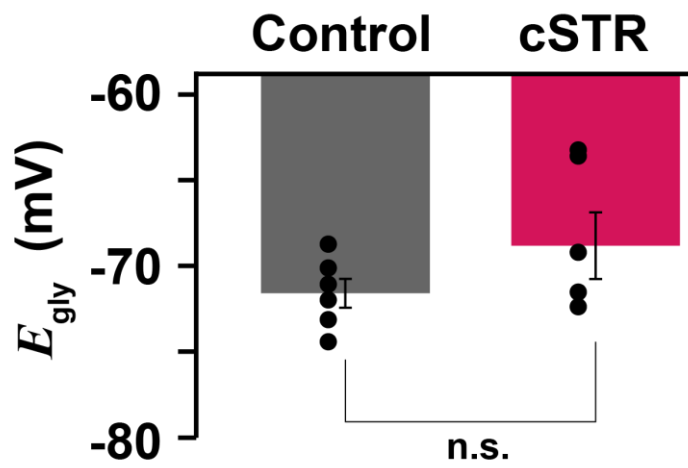
Figure 12

Figure 13. Voltage-clamp recording of miniature glycinergic currents

(A) Protocol for electrophysiological patch-clamp recording. In order to exclude the effect of strychnine residue, extracellular solution of both control and chronic strychnine treatment groups was exchanged to 1 μM strychnine for 30 seconds, and then completely exchanged to strychnine-lacking solution. The voltage-clamp recordings were started within 10 minutes after strychnine washout.

(B) Representative traces of miniature glycinergic currents under voltage clamp configuration (V_H: -70 mV) in the presence of TTX, CNQX, AP-V, SR95531. After each recording, the responses were confirmed as strychnine-sensitive currents by strychnine.

(C) Representative examples of cumulative plots in control and cSTR wash groups shown in panel B. Each trace was plotted by total miniature currents during 180 seconds.

(D) (E) Average normalized amplitudes (D) and frequencies (E) of control (filled circles, n=5) and cSTR wash (open circles, n=5) groups in each time points after cSTR removal (Mean ± SEM).
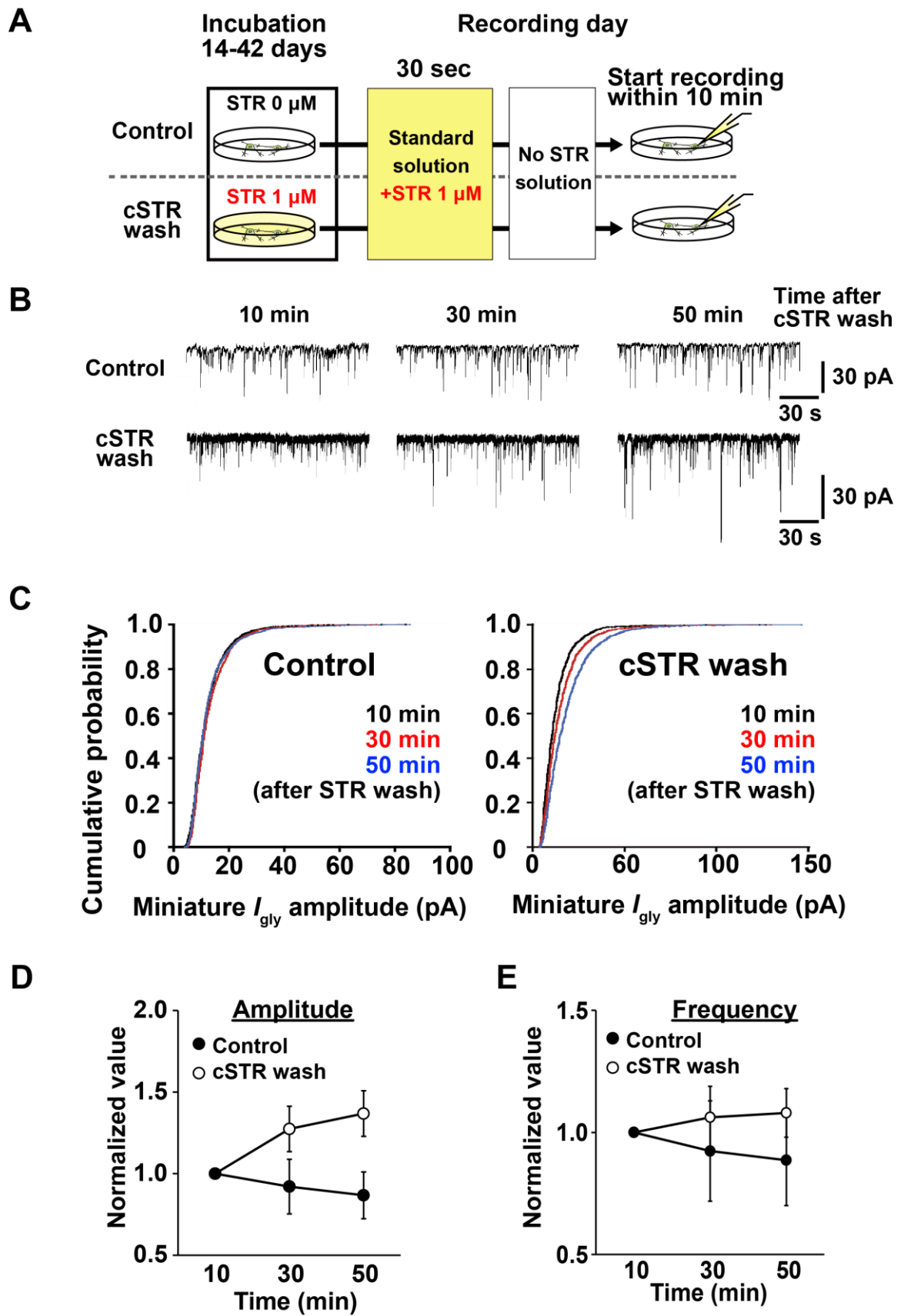
Figure 13

Figure 14. Activation-dependent GlyR dynamics at synapse

(A) Schematic illustration indicating that activated GlyR with lower lateral diffusion and inactivated GlyR with higher lateral diffusion. Longer dwelling time with lower diffusion property, activated GlyRs specifically accumulate at synapses.

A
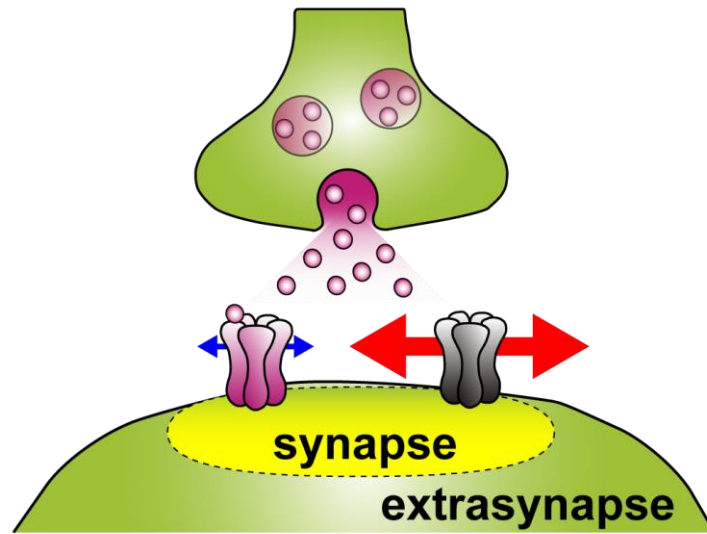
GlyR activation

↓

Lower lateral diffusion

↓

Concentrated GlyRs localization at synapses

Chronic GlyR blockade

↓

Higher lateral diffusion

↓

Dispersed GlyRs localization

Figure 14

Acknowledgements

Finally, I also would like to thank all members of Division of Homeostatic Development in National Institute of Physiological Sciences for their supports and kindnesses.